nagra.

Technical Report 17-05

Chemistry of selected dose-relevant radionuclides

March 2017

W. Hummel

Paul Scherrer Institut, Villigen PSI

National Cooperative
for the Disposal of
Radioactive Waste

Hardstrasse 73
CH-5430 Wettingen
Switzerland
Tel. +41 56 437 11 11

www.nagra.ch

nagra.

Technical Report 17-05

Chemistry of selected dose-relevant radionuclides

March 2017

W. Hummel

Paul Scherrer Institut, Villigen PSI

National Cooperative
for the Disposal of
Radioactive Waste

Hardstrasse 73
CH-5430 Wettingen
Switzerland
Tel. +41 56 437 11 11

www.nagra.ch

ISSN 1015-2636

"Copyright © 2017 by Nagra, Wettingen (Switzerland) / All rights reserved.
All parts of this work are protected by copyright. Any utilisation outwith the remit of the copyright law is unlawful and liable to prosecution. This applies in particular to translations, storage and processing in electronic systems and programs, microfilms, reproductions etc."

Abstract

When looking at the dose rate calculations made as part of the provisional safety assessment in Stage 2 of the Sectoral Plan (Nagra 2014a), it is remarkable that only very few radionuclides contribute to the resulting dose rate. These radionuclides include C-14 (instant and congruent release), Cl-36, Se-79 and I-129. The reasons for this observation are the limited retardation of these radionuclides in clay- and cement-based environment and/or their unknown chemical speciation. This report gathers information regarding inventory, chemical speciation in the relevant waste sorts and transport processes in clay and/or cement (sorption and diffusion). This is done for each of the following radionuclides: Cl-36, Se-79, Ag-108m and I-129. As the research on C-14 speciation and retardation is ongoing, a separate report will deal with the contribution of C-14. Based on existing literature, the report investigates the origins of uncertainties, describes the complexity and nature of the waste in which the radionuclides are formed, evaluates the possible speciation for each element and makes suggestions of how the remaining uncertainties can be reduced in the future. The report comes to the conclusion that uncertainties in the inventory or in the speciation for Cl-36, Se-79 and Ag-108m could be further reduced by dedicated studies. For Cl-36, verifying the inventory of Cl-36 in spent fuel, cladding and stainless steel can decrease the dose contribution. In case of Se-79, thermodynamic and modelling exercises to understand the Se(cr) ⇌ Se(aq) system and the uptake of Se in sulphides can reduce the dose contribution. A similar study on the Ag(cr) ⇌ Ag(aq) system could also elucidate the speciation and solubility of Ag-108m. Finally, this report however estimates the chance of reducing the dose rate contribution of I-129 by doing further studies as very low, as the chemical speciation and the inventory are well-known and have been extensively characterised.

Zusammenfassung

Bei Betrachtung der Berechnungen der Dosisraten, die als Teil der provisorischen Sicherheitsanalysen in Etappe 2 des Sachplans geologische Tiefenlager durchgeführt wurden (Nagra 2014a), fällt auf, dass lediglich sehr wenige Radionuklide zur resultierenden Dosisrate beitragen. Bei diesen Radionukliden handelt es sich um C-14 (instantane und kongruente Freisetzung), Cl-36, Se-79 und I-129. Die Gründe für eine solche Beobachtung liegen in der begrenzten Rückhaltung dieser Radionuklide in einem ton- und zementbetontem Barrierensystem und/oder deren unbekannter Speziation. Der vorliegende Bericht stellt Informationen zum Inventar, zur chemischen Speziation in der relevanten Abfallsorte und zu Transportprozessen in Ton(stein) und/oder Zement (Sorption und Diffusion) für die folgenden Radionuklide zusammen: Cl-36, Se-79, Ag-108m und I-129. Die Untersuchung der Speziation und Rückhaltung von C-14 ist Gegenstand laufender Forschungsprojekte und wird in einem separaten Bericht behandelt. Basierend auf vorhandener Literatur werden im vorliegenden Bericht die Herkunft von Ungewissheiten untersucht, die Komplexität und Art der Radionuklid-haltigen Abfälle beschrieben, die mögliche Speziation für jedes Radionuklid evaluiert und Möglichkeiten zur künftigen Reduktion der verbleibenden Ungewissheiten vorgeschlagen. Der Bericht gelangt zur Erkenntnis, dass die Ungewissheiten bezüglich Inventar oder Speziation für Cl-36, Se-79 und Ag-108m durch geeignete Untersuchungen weiter reduziert werden könnten. Bei Cl-36 kann die Überprüfung dessen Inventars in abgebrannten Brennelementen, Hüllrohren und rostfreiem Stahl den Dosisbeitrag senken. Für Se-79 können thermodynamische Betrachtungen sowie Modellierungen im Hinblick auf das Verständnis des Systems Se(cr) ⇌ Se(aq) und die Aufnahme von Se in Sulfiden den Dosisbeitrag reduzieren. Eine ähnliche Studie zum System Ag(cr) ⇌ Ag(aq) könnte zudem zur Bestimmung der Speziation und Löslichkeit von Ag-108m beitragen. Letztlich wird im Bericht allerdings die Möglichkeit, den Dosisbeitrag von I-129 durch weitere Studien zu reduzieren als sehr gering eingeschätzt, da die chemische Speziation und das Inventar gut bekannt sind und bereits ausführlich beschrieben wurden.

Résumé

Si l'on considère les résultats des calculs de dose effectués dans le cadre de l'étude de sûreté préliminaire présentée à l'étape 2 du Plan sectoriel (Nagra 2014a), on observe que seul un très petit nombre de radionucléides contribue aux débits de dose obtenus. Parmi ces radionucléides figurent C-14 (relâchement instantané et congruent), Cl-36, Se-79 et I-129. Cette constatation peut s'expliquer par le fait que, dans un environnement dominé par l'argile ou le ciment, ces radionucléides sont peu retardés, et/ou parce que l'on ignore leur spéciation chimique. Le présent rapport rassemble des informations sur l'inventaire, la spéciation chimique dans les types de déchets concernés et les processus de transfert dans l'argile et/ou le ciment (sorption et diffusion) – ceci pour les radionucléides suivants : Cl-36, Se-79, Ag-108m et I-129. Les recherches sur la spéciation et le retard de C-14 sont actuellement en cours, de sorte que le rapport correspondant sera publié séparément. Sur la base des publications existantes, le présent rapport étudie les origines des incertitudes, décrit la complexité et la nature des déchets d'où proviennent les radionucléides, estime la spéciation potentielle de chaque élément et suggère des pistes de recherche pour parvenir à réduire les incertitudes. Le rapport conclut que des études spécifiques permettrait de réduire encore les incertitudes relatives à l'inventaire et à la spéciation de Cl-36, Se-79 et Ag-108m. Dans le cas de Cl-36, le fait de vérifier l'inventaire de Cl-36 dans les éléments combustibles usés, les gaines et l'acier inoxydable permettrait de réduire sa contribution au débit de dose. Concernant Se-79, des essais thermodynamiques et de modélisation portant sur le système Se(cr) ⇌ Se(aq) et l'absorption du Se par les sulfures peuvent réduire leur impact sur le débit de dose. Une étude similaire du système Ag(cr) ⇌ Ag(aq) permettrait également de clarifier la spéciation et la solubilité de Ag-108m. Enfin, pour I-129, le présent rapport doit cependant conclure que des études supplémentaires ont très peu de chances de réduire sa contribution au débit de dose, car sa spéciation chimique et son inventaire sont bien connus et ont été largement caractérisés.

Table of Contents

List of Tables

List of Figures

1 Introduction

1.1 Background

As part of the safety case and the provisional safety assessment (Nagra 2014a), dose calculations are made to assess the dose rate that is released from the high level waste (HLW) or from the low and intermediate level waste (L/ILW) repository. Such dose calculations are typically made for a certain set of radionuclides. The reason for this is that the waste inventory contains many radionuclides that either have a short half-life or are present at very low concentrations. This set of radionuclides is called dose-relevant radionuclides[1]. In Nagra (2014a) the list of dose-relevant radionuclides for each repository (HLW and L/ILW) is presented. For all radionuclides on this list, solubility products, sorption and diffusion coefficients in the cementitious or bentonite near field and sorption and diffusion coefficients in the far field have been acquired and serve as input for the dose-calculations (Baeyens et al. 2014, Berner 2014a, 2014b, Wieland 2014, Van Loon 2014).

Among this set of dose-relevant radionuclides, some radionuclides contribute disproportionally to the total dose rate because their inventory is unclear, their speciation is not well-understood or no diffusion or sorption coefficients are known. As can be seen in Fig. 1 the total dose rate for a HLW repository at the site Jura Ost (JO) is largely defined by radionuclides such as C-14 (congruently released organic C-14 is indicated as Ch-14C, instantaneous released C-14 is indicated as Ch-14), Cl-36, Se-79 and I-129.

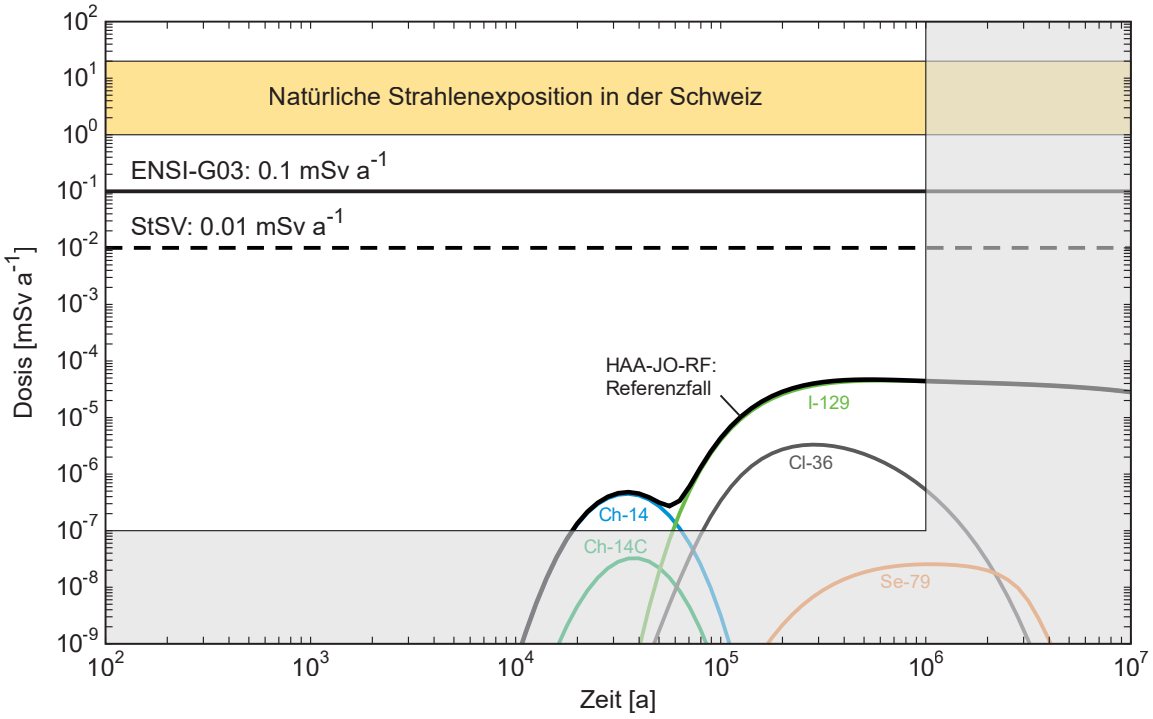

Fig. 1: Total dose rate for a HLW repository at the site Jura Ost (JO) (Nagra 2014a).

[1] Previously, these radionuclides were called "safety-relevant" radionuclides. However, as these radionuclides are selected for dose-calculations in contrast to other calculations, the terminology dose-relevant is preferred. In contrast to dose-calculations, other safety-related analysis might require other sets of radionuclides (e.g. operational safety, chemotoxicity).

The aim of this report is to take a closer look at the inventory and chemistry of some of these dose-relevant radionuclides that contribute significantly to the overall dose rate. By identifying possibilities to reduce uncertainties in the nuclide inventory or speciation, the dose rates can potentially be further reduced.

1.2 Generation of radionuclides in radioactive waste

Besides the selection procedure applied in Nagra (2014a), an attempt is made to identify dose-relevant radionuclides for the Swiss geological repository project, starting from generic considerations, then adding more case specific criteria.

As a starting point for the identification of dose-relevant radionuclides, we take a closer look at the different processes through which radionuclides can be produced in a nuclear reactor. Thermal neutrons in a nuclear reactor produce radioactive isotopes mainly by

1. Fission of U-235 and Pu-239 (fission products)
2. Neutron capture by U-238 and β^- decay (transuranium elements)
3. Neutron activation of structural material (activation products)

While most activation products decay in one or few steps to stable daughter products, actinides (uranium and transuranium elements) decay in long decay chains via many radioactive daughter products (actinide decay products) into stable isotopes.

In addition to radioactive isotopes produced in nuclear power plants radioactive waste also contains radioactive isotopes originating from Medicine, Industry and Research (MIR waste). However, the discussion of MIR waste is outside the scope of this report.

Fission products

Because the highest radioactivity in radioactive waste comes from spent nuclear fuel – which consists of UO_2 or mixed oxides (MOX) in which Pu-239 is added to U-235 – this waste forms a good starting point to consider the selection of dose-relevant radionuclides.

Fission of ^{235}U by thermal neutrons in light water reactors is a stochastic process resulting in a large number of fission products. The amounts of fission products are characterised by their independent fission yield, usually given in % (or the number of nuclides produced in 100 fission reactions). While most fission reactions produce two fission products, generally of different masses, rare events produce three fission products (ternary fission) where the third nuclide has a low atomic mass from ^{1}H to ^{21}Ne. These ternary fission events occur on average two times in 1'000 fission reactions. Therefore, the total independent fission yield for ^{235}U is not exactly 200.0 % but 200.2 %.

The vast majority of the 977 fission products listed for fission of ^{235}U by thermal neutrons in www.nucleonica.net, JEFF-3.1 database, have very short half-lives ($T_{1/2}$) in the range of milliseconds (30 %), seconds (28 %) and minutes (16 %). They all decay quickly into longer lived or stable isotopes.

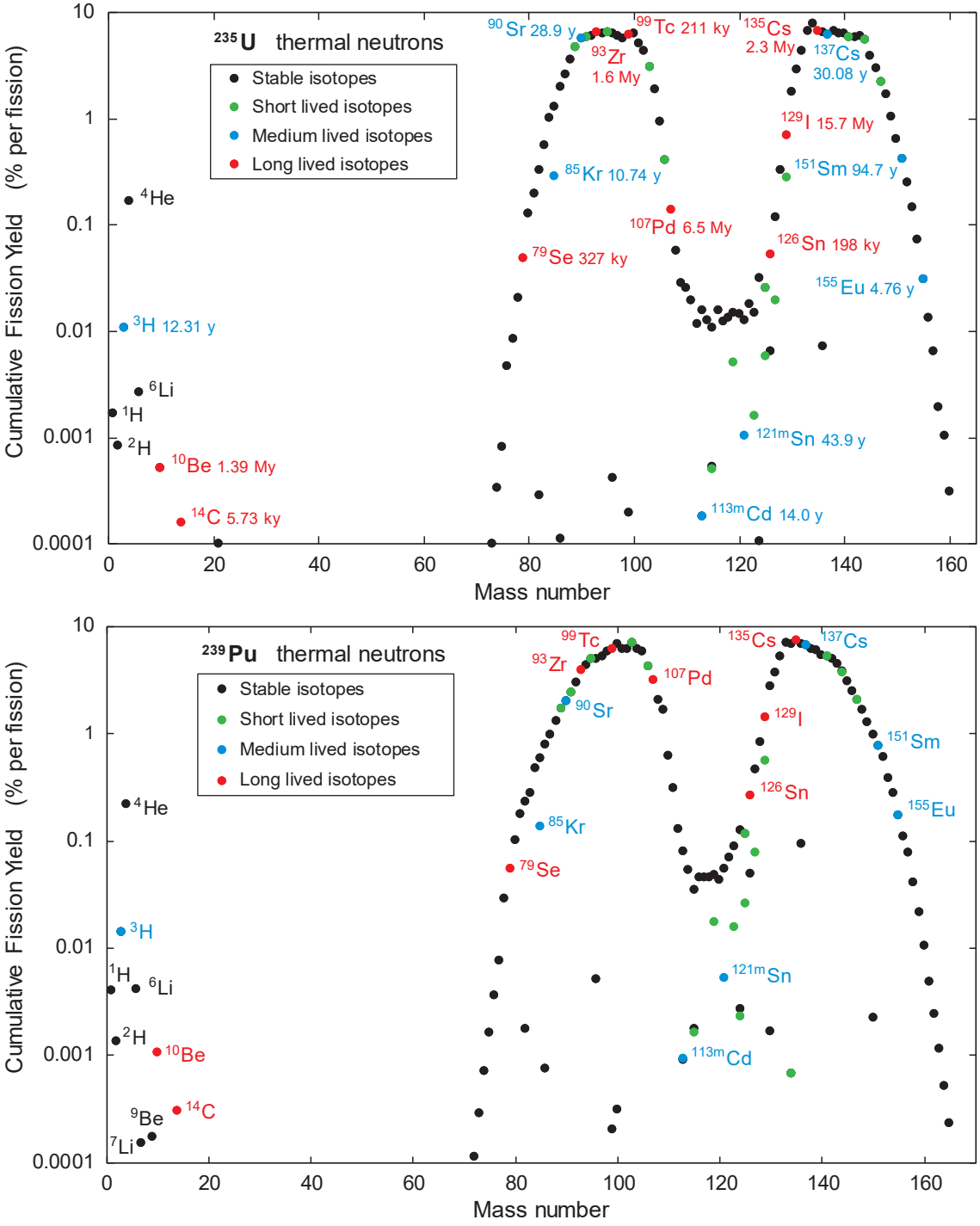

Fig. 2: Cumulative fission yield (%) of ^{235}U and ^{239}Pu fission with thermal neutrons, i.e. the total number of atoms of a specific nuclide produced (directly and via decay of precursors) in 100 fission reactions.

Data taken from www.nucleonica.net, Karlsruhe Nuclide Chart Online, KNCO++. Stable isotopes: Stable or $T_{1/2} > 1.4 \times 10^{10}$ years, the half-life of ^{232}Th or the age of the universe. Short lived isotopes: 30 days < $T_{1/2}$ < 3 years, significant decay in 40 years interim storage. Medium lived Isotopes: 3 years < $T_{1/2}$ < 100 years, complete decay in 10'000 years in a canister. Long lived isotopes: $T_{1/2}$ > 5'000 years. There are no fission products with half-lives between 100 and 5'000 years and cumulative fission yield > 0.0001 %.

Hence, the independent fission yield is not relevant for waste management considerations. There we need the cumulative fission yield, i.e. the total number of atoms of a specific nuclide produced directly and via decay of precursors in 100 fission reactions.

The cumulative fission yield for fission products of ^{235}U with half-lives longer than 30 days and fission yields higher than 0.0001 % is shown in Fig. 2 (top). The number of fission products is now considerably smaller: 97 stable isotopes, 16 short lived isotopes (30 days < $T_{1/2}$ < 3 years), 8 medium lived isotopes (3 years < $T_{1/2}$ < 100 years) and 9 long lived isotopes ($T_{1/2}$ > 5'000 years). There are no fission products with half-lives between 100 and 5'000 years and cumulative fission yield > 0.0001 %.

The numbers for ^{239}Pu fission with thermal neutrons are similar (Fig. 2, bottom): 107 stable isotopes, 18 short lived, 8 medium lived and 9 long lived isotopes. The distributions of cumulative fission yields versus mass number also look similar with their characteristic "twin peaks" due to asymmetric binary fission products. The cumulative fission yields are slightly different for ^{235}U and ^{239}Pu fission and so the inventories of fission products from spent UO_2 fuel and spent MOX fuel are slightly different.

If we look at cumulative fission yields above 0.001 % for ^{235}U and ^{239}Pu we have 7 long-lived fission products (Se-79, Zr-93, Tc-99, Pd-107, Sn-126, I-129, Cs-135) and 7 medium-lived fission products (H-3, Kr-85, Sr-90, Sn-121m, Cs-137, Sm-151, Eu-155). These are generic candidates for dose-relevant radionuclides. Be-10, C-14 and Cd-113m are not important as fission products because they have a low cumulative fission yield, but they are also produced by neutron activation in a nuclear reactor.

Concerning the chemistry of dose-relevant nuclides, the fission gases tritium (^{3}H) and krypton (^{85}Kr) are not discussed here, and we are left with 12 radionuclides or 10 elements from nuclear fission: Se, Sr, Zr, Tc, Pd, Sn, I, Cs, Sm and Eu.

Transuranium elements

The non-fissile ^{238}U also contributes radionuclides to the list of dose- relevant ones. ^{238}U can capture a neutron and form ^{239}U, which is a β^- active nuclide. It decays with a half-life of 23.5 minutes into ^{239}Np, which is the first transuranium element. ^{239}Np is also β^- active and decays with a half-life of 2.355 days into ^{239}Pu:

$$^{238}U + {}^{1}n \rightarrow {}^{239}U \rightarrow {}^{239}Np + \beta^- \rightarrow {}^{239}Pu + \beta^-$$

Also the fissile ^{235}U sometimes captures a neutron to form ^{236}U which is not split into fission products. ^{236}U in turn can capture a neutron and form ^{237}U, which is a β^- active nuclide. It decays with a half-life of 6.75 days into ^{237}Np, a long-lived isotope:

$$^{235}U + {}^{1}n \rightarrow {}^{236}U + {}^{1}n \rightarrow {}^{237}U \rightarrow {}^{237}Np + \beta^-$$

Likewise the fissile ^{239}Pu sometimes captures a neutron to form ^{240}Pu without being split into fission products. Repeated neutron capture leads to ^{241}Pu, ^{242}Pu and ^{243}Pu. The latter is a β^- active nuclide. It decays with a half-life of 4.956 hours into ^{243}Am, another long-lived isotope.

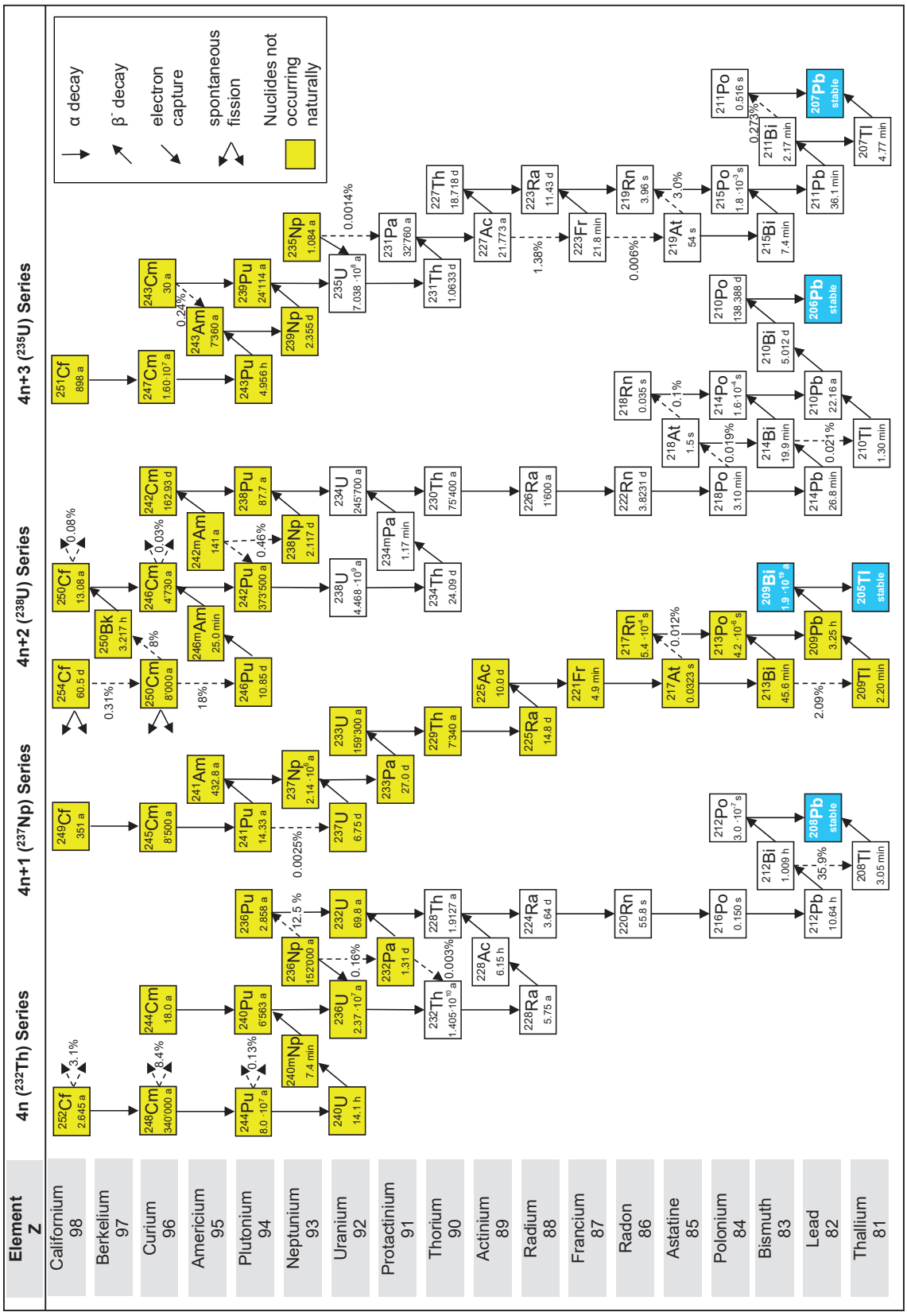

Fig. 3: Decay chains of actinides in spent nuclear fuel.

Data taken from www.nucleonica.net, Karlsruhe Nuclide Chart Online, KNCO++.

Hence, by repeated neutron capture and subsequent beta decays the transuranium elements Np, Pu, Am, Cm and Cf are produced in a nuclear reactor. Together with the naturally occurring Th and U, this group of elements is called actinides, after Actinium (Ac), the first element of this group in the periodic table.

Actinide decay products

All these actinides decay in four different decay chains (Fig. 3) via many steps to finally stable ^{206}Pb, ^{207}Pb, ^{208}Pb and ^{209}Bi (actually, ^{209}Bi decays with a half-life of 1.9×10^{19} years to ^{209}Tl, but still can be considered as "stable").

Some of the longer lived decay products in these decay chains, with half-lives longer than 100 days, are also potentially dose- relevant, i.e. Pa-231, Th-228, Th-229, Th-230, Th-232, Ac-227, Ra-226, Ra-228, Po-210 and Pb-210 (Fig. 3). This adds 10 radionuclides or six elements to the list of potentially dose- relevant ones: Pa, Th, Ac, Ra, Po and Pb.

Activation products

Last but not least, thermal neutrons in a nuclear reactor are captured by many stable nuclides in the structural material of the reactor. This "neutron activation" processes produce many radionuclides. Some of them are long-lived enough and produced in such amounts that they become dose-relevant in geological repositories.

Important long-lived activation products in reactor materials, with half-lives longer than 100 years and sufficient production to become potentially dose-relevant, are (Evans et al. 1984): Be-10, C-14, Cl-36, Ca-41, Ni-59, Ni-63, Se-79, Zr-93, Nb-94, Mo-93, Ag-108m, Ho-166m. Two of these activation products are also produced in dose-relevant quantities by fission: Se-79 and Zr-93. This leaves 10 radionuclides or nine elements produced mainly by neutron activation: Be, C, Cl, Ca, Ni, Nb, Mo, Ag and Ho.

Selection of dRN

All of these radionuclides or elements (with the exception of Cf) have been considered as dose-relevant in previous safety analyses (Nagra 2014a) and some geochemical key properties of them are given in Tab. 1. From this table it is clear that for some radionuclides none or little sorption, solubility or diffusion data is available. These radionuclides include: C-14, Cl-36, Se-79, Ag-108m and I-129. As a result, these dose-relevant radionuclides will contribute more to the final dose rate than those with reliable and sufficient retention properties.

The aim of this report is to describe the repository-relevant chemistry of the abovementioned radionuclides. From these radionuclides, C-14 is not dealt with in this report. The current state of knowledge about C-14 has been discussed by Wieland & Hummel (2015) and research projects concerning organic molecules containing C-14 are ongoing, at PSI/LES and elsewhere (e.g. Swissnuclear, EU-project CAST). So, it was decided not to include C-14 in the present report. For the other 4 radionuclides, which are discussed according to atomic weight in the following chapters, no "general chemistry of everything" has been reviewed, but (geo)chemical aspects related to the Swiss safety case are discussed here.

Tab. 1: Geochemical data used in provisional safety analyses for SGT-E2.

Sorption data for Opalinus Clay (reference case) and MX-80 bentonite (reference case) taken from Baeyens et al. (2014). Sorption data for hardened cement paste (HCP, Stage I, reducing conditions) taken from Wieland (2014). Diffusion data for Opalinus Clay (reference case, 25 °C) and for compacted bentonite (reference case, 25 °C) taken from Van Loon (2014). Solubility data (reference case) for a bentonite environment and a cementitious near field (ILW 1) taken from Berner (2014a, 2014b: Appendix A).

Element	Sorption				Diffusion		Solubility	
	Opalinus Clay	Bentonite	Cement		Opalinus Clay	Bentonite	Bentonite	Cement
	R_d [$m^3 \cdot kg^{-1}$]	R_d [$m^3 \cdot kg^{-1}$]	R_d [$m^3 \cdot kg^{-1}$]		D_e [$m^2 \cdot s^{-1}$]	D_e [$m^2 \cdot s^{-1}$]	[$mol \cdot kg^{-1}$]	[$mol \cdot kg^{-1}$]
Be(II)	1.33	2.29	0		$4.9 \cdot 10^{-12}$	$6.8 \cdot 10^{-11}$	$9 \cdot 10^{-7}$	$2 \cdot 10^{-4}$
C_{inorg}	0.00143	0.00006	isotopic exch.	anion	$1.7 \cdot 10^{-12}$	$1.4 \cdot 10^{-12}$	$9 \cdot 10^{-4}$	$8 \cdot 10^{-6}$
C_{org}	0	0	0.0001		$1.1 \cdot 10^{-11}$	$1.8 \cdot 10^{-10}$	–	–
Cl(-I)	0	0	0.005	anion	$2.4 \cdot 10^{-12}$	$2.0 \cdot 10^{-12}$	not limited	not limited
K(I)	0.00505	0.00713	0.0001		$1.0 \cdot 10^{-10}$	$6.3 \cdot 10^{-10}$	-	not limited
Ca(II)	0.00063	0.00233	-		$1.0 \cdot 10^{-11}$	$1.3 \cdot 10^{-10}$	$9 \cdot 10^{-3}$	-
Co(II)	0.672	0.415	isotopic exch.		$4.9 \cdot 10^{-12}$	$6.8 \cdot 10^{-11}$	-	$5 \cdot 10^{-7}$
Ni(II)	1.34	1.28	isotopic exch.		$4.9 \cdot 10^{-12}$	$6.8 \cdot 10^{-11}$	$6 \cdot 10^{-5}$	$3 \cdot 10^{-6}$
Se(-II)	0	0	-	anion	$1.3 \cdot 10^{-12}$	-	$5 \cdot 10^{-9}$	$2 \cdot 10^{-6}$
Se(IV)	-	-	0.03	anion	-	$1.1 \cdot 10^{-12}$	-	-
Sr(II)	0.00064	0.00233	0.1		$1.8 \cdot 10^{-11}$	$2.1 \cdot 10^{-10}$	$1 \cdot 10^{-4}$	$2 \cdot 10^{-3}$
Zr(IV)	125	1020	10		$4.9 \cdot 10^{-12}$	$6.8 \cdot 10^{-11}$	$1 \cdot 10^{-7}$	$5 \cdot 10^{-9}$
Nb(V)	1.0	1.0	1		$4.9 \cdot 10^{-12}$	$6.8 \cdot 10^{-11}$	$7 \cdot 10^{-5}$	not limited
Mo(VI)	0.00378	0.0133	0	anion	$1.3 \cdot 10^{-12}$	$1.1 \cdot 10^{-12}$	$2 \cdot 10^{-5}$	$7 \cdot 10^{-6}$
Tc(IV)	1.19	3.38	1		$4.9 \cdot 10^{-12}$	$6.8 \cdot 10^{-11}$	$4 \cdot 10^{-9}$	$2 \cdot 10^{-6}$
Pd(II)	0.323	0.578	-		$4.9 \cdot 10^{-12}$	$6.8 \cdot 10^{-11}$	$6 \cdot 10^{-8}$	-
Ag(I)	0	0	0		$1.1 \cdot 10^{-11}$	$1.8 \cdot 10^{-10}$	$1 \cdot 10^{-5}$	$2 \cdot 10^{-6}$
Sn(IV)	103	813	10		$4.9 \cdot 10^{-12}$	$6.8 \cdot 10^{-11}$	$9 \cdot 10^{-8}$	$1 \cdot 10^{-7}$
I(-I)	0	0	0.001	anion	$2.4 \cdot 10^{-12}$	$2.0 \cdot 10^{-12}$	not limited	not limited
Cs(I)	2.04	0.0293	0.0005		$1.7 \cdot 10^{-10}$	$8.3 \cdot 10^{-10}$	not limited	not limited
Sm(III)	15.0	31.6	100		$4.9 \cdot 10^{-12}$	$6.8 \cdot 10^{-11}$	$2 \cdot 10^{-7}$	$5 \cdot 10^{-7}$
Eu(III)	5.91	13.1	100		$4.9 \cdot 10^{-12}$	$6.8 \cdot 10^{-11}$	–	$2 \cdot 10^{-6}$
Ho(III)	10.5	25.1	-		$4.9 \cdot 10^{-12}$	$6.8 \cdot 10^{-11}$	$3 \cdot 10^{-6}$	–
Pb(II)	7.03	9.54	0.5		$4.9 \cdot 10^{-12}$	$6.8 \cdot 10^{-11}$	$9 \cdot 10^{-7}$	$5 \cdot 10^{-3}$
Po(IV)	0.528	1.20	0		$4.9 \cdot 10^{-12}$	$6.8 \cdot 10^{-11}$	$7 \cdot 10^{-7}$	$6 \cdot 10^{-8}$
Ra(II)	0.00044	0.00128	0.5		$1.4 \cdot 10^{-11}$	$1.5 \cdot 10^{-10}$	$3 \cdot 10^{-10}$	$1 \cdot 10^{-6}$
Ac(III)	7.25	7.56	100		$4.9 \cdot 10^{-12}$	$6.8 \cdot 10^{-11}$	$3 \cdot 10^{-6}$	$2 \cdot 10^{-6}$
Th(IV)	35.8	76.9	100		$4.9 \cdot 10^{-12}$	$6.8 \cdot 10^{-11}$	$4\ 10^{-9}$	$1 \cdot 10^{-9}$
Pa(V)	33.0	75.3	100		$4.9 \cdot 10^{-12}$	$6.8 \cdot 10^{-11}$	$5\ 10^{-9}$	$2 \cdot 10^{-6}$
U(IV)	0.198	0.371	100		$4.9 \cdot 10^{-12}$	$6.8 \cdot 10^{-11}$	-	-
U(VI)	0.00037	0.00009	-		$4.9 \cdot 10^{-12}$	$6.8 \cdot 10^{-11}$	$2 \cdot 10^{-7}$	$7 \cdot 10^{-7}$
Np(IV)	132	375	100		$4.9 \cdot 10^{-12}$	$6.8 \cdot 10^{-11}$	$1 \cdot 10^{-8}$	$1 \cdot 10^{-9}$
Pu(III)	7.24	62.4	100		$4.9 \cdot 10^{-12}$	$6.8 \cdot 10^{-11}$	$7 \cdot 10^{-10}$	-
Pu(IV)	0.0343	0.0938	100		$4.9 \cdot 10^{-12}$	$6.8 \cdot 10^{-11}$	-	$2 \cdot 10^{-12}$
Am(III)	7.25	7.56	100		$4.9 \cdot 10^{-12}$	$6.8 \cdot 10^{-11}$	$3 \cdot 10^{-6}$	$5 \cdot 10^{-10}$
Cm(III)	7.25	7.56	100		$4.9 \cdot 10^{-12}$	$6.8 \cdot 10^{-11}$	$4 \cdot 10^{-6}$	$1 \cdot 10^{-9}$
							faster diffusion	

	illite	montmorillonite	HCP	source data
				set to zero
				chemical analogue
				special cases

1.3 Inventory of the selected dose-relevant radionuclides

A first look at the radioactive waste inventory, MIRAM 14 (Nagra 2014b) reveals that the vast majority of activity from these 4 selected radionuclides is concentrated in few waste forms (Tab. 2). The waste forms explicitly listed in Tab. 2 count for more than 99.9 % activity (or mole percent) in the cases of Se-79, I-129 and Ag-108m and for about 95 % in the case of Cl-36.

High-**L**evel **W**aste comprising **S**pent nuclear **F**uel (HLW SF) from the Swiss nuclear power plants contains some or even the majority of the activity of all selected radionuclides, i.e. Se-79, I-129, Cl-36 and Ag-108m (Tab. 2).

Considerable activity of three of the selected radionuclides is found in each of these waste types as defined by KEG (Tab. 2):

- Vitrified **H**igh-**L**evel **W**aste from reprocessing of spent nuclear fuel (HLW vitrified)
- **A**lpha-**T**oxic **W**aste (ATW), also called long-lived **I**ntermediate-**L**evel **W**aste from reprocessing (ILW reprocess), mainly compacted hulls and ends and vitrified sludges
- **L**ow- and **I**ntermediate-**L**evel **W**aste (L/ILW) from decommissioning in the form of stainless steel from reactor internals (L/ILW steel)

Finally, two element specific cases can be identified (Tab. 2):

- In the case of I-129, the main **L**ow- and **I**ntermediate-**L**evel **W**aste (L/ILW) form comprises **I**on-**E**xchange **R**esins (IER).
- In the case of Ag-108m, the large majority of activity (98.2 %) is found in a single waste form containing metallic silver, Ag(0).

1.4 Structure of the report

Each chapter begins with "origin and initial waste forms": This is the "source term", i.e. how the radionuclide is produced, in which chemical state (if known), and in which waste containers. The latter aspect is important if the repository is no longer considered as a "global mixing tank" in safety assessments, but the chemistry of specific waste forms will be modelled.

Then, some general chemical knowledge and recent research results concerning the retardation of the radionuclide with respect to safety cases of Swiss geological repositories is elucidated. Just the (geo)chemical aspects are discussed, no reactive transport modelling and no full-fledged safety assessments are considered here.

The final chapter, "future research needs" is a heavily biased view of a geochemist interested in furthering fundamental knowledge of retardation mechanisms.

Tab. 2: Distribution of ^{79}Se, ^{129}I, ^{36}Cl and ^{108m}Ag to different waste forms in mole percent (or activity percent) according to MIRAM 14 (Nagra 2014b).

The abbreviations are HLW SF: **H**igh-**L**evel **W**aste comprising **S**pent nuclear **F**uel assemblies. HLW vitrified: vitrified **H**igh-**L**evel **W**aste from reprocessing of spent fuel. ILW reprocess: long-lived **I**ntermediate-**L**evel **W**aste from reprocessing (compacted hulls and ends, vitrified sludges). L/ILW: **L**ow- and **I**ntermediate-**L**evel **W**aste. steel: decommissioning waste, stainless steel from reactor internals. IER: Ion-**E**xchange **R**esins. plasma: waste incinerated in the ZWILAG plasma plant. Ag(0): metallic silver.

The waste form codes are taken from Nagra (2014a, Tab. A3.1-7).

Se-79	**I-129**	**Cl-36**	**Ag-108m**
HLW SF 47.92 % BE-L-UO2-U-HAA BE-G-UO2-U-HAA BE-B-UO2-U-HAA BE-M-UO2-U-HAA BE-G-MOX-U-HAA BE-B-MOX-U-HAA	**HLW SF 99.52 %** BE-L-UO2-U-HAA BE-G-UO2-U-HAA BE-B-UO2-U-HAA BE-M-UO2-U-HAA BE-G-MOX-U-HAA BE-B-MOX-U-HAA	**HLW SF 60.87 %** BE-L-UO2-U-HAA BE-G-UO2-U-HAA BE-B-UO2-U-HAA BE-M-UO2-U-HAA BE-G-MOX-U-HAA BE-B-MOX-U-HAA	HLW SF 1.11 % BE-L-UO2-U-HAA BE-G-UO2-U-HAA BE-B-UO2-U-HAA BE-M-UO2-U-HAA BE-G-MOX-U-HAA BE-B-MOX-U-HAA
HLW vitrified 51.58 % WA-F-KG-K1-HAA WA-U-KG-K1-HAA	HLW vitrified 0.38 % WA-F-KG-K1-HAA WA-U-KG-K1-HAA		HLW vitrified 0.13 % WA-U-KG-K1-HAA WA-F-KG-K1-HAA
ILW reprocess 0.244 % WA-F-MX-K1-ATA WA-F-SG-K1-ATA	ILW reprocess 0.075 % WA-F-MX-K1-ATA WA-F-SG-K1-ATA	**ILW reprocess 9.23 %** WA-F-MX-K1-ATA WA-F-SG-K1-ATA	
			ILW Ag(0) 0.23 % SA-LU-MX-L3-ATA
ILW others 0.009 %	ILW others 0.011 %	ILW others 0.78 %	ILW others 0.01 %
			L/ILW Ag(0) 98.23 % RA-B-MX-M2-SMA RA-G-MX-M2-SMA
			L/ILW plasma 0.17 % BA-Z-PA-C1-SMA
L/ILW steel 0.243 % SA-B-ME-M2-SMA SA-G-ME-M2-SMA SA-M-ME-M2-SMA SA-L-ME-M2-SMA		**L/ILW steel 24.71 %** SA-B-ME-M2-SMA SA-G-ME-M2-SMA SA-M-ME-M2-SMA SA-L-ME-M2-SMA	L/ILW steel 0.08 % SA-G-ME-M2-SMA SA-B-ME-M2-SMA SA-M-ME-M2-SMA SA-L-ME-M2-SMA
	L/ILW IER 0.015 % SA-M-H-M2-SMA BA-M-H-F2-SMA SA-L-H-M2-SMA BA-L-H-F2-SMA BA-B-HP-F2-SMA BA-B-HP-F1-SMA BA-G-HB-F2-SMA SA-B-H-M2-SMA SA-G-H-M2-SMA		
		L/ILW other metals 2.85 %	
L/ILW others 0.008 %	L/ILW others 0.001 %	L/ILW others 1.56 %	L/ILW others 0.04 %
Total 99.50 % Total 99.98 %	**99.52 %** 99.99 %	**94.81 %** 94.81 %	**98.23 %** 99.95 %

2 Cl-36

2.1 Origin and initial waste forms

Chlorine has two stable isotopes, ^{35}Cl and ^{37}Cl, with natural abundances of 75.76 % and 24.24 %, respectively, and one long-lived radioactive isotope, ^{36}Cl, with a half-life of $(3.013 \pm 0.015) \times 10^5$ years. All other radioactive chlorine isotopes have half-lives of minutes or less.

In a nuclear reactor ^{36}Cl is produced by neutron capture of the stable nuclide ^{35}Cl. The reaction $^{35}Cl + {}^{1}n \rightarrow {}^{36}Cl + \gamma$ is characterized by a high cross section of 43.63 barn. Thus, even trace amounts of ^{35}Cl in nuclear fuel and structural reactor material are sufficient to produce significant amounts of ^{36}Cl, provided that we have a sufficient flux of thermal neutrons.

Trace amounts of radioactive ^{36}Cl exist in the environment, in a ratio of about $(7\text{-}10) \times 10^{-13}$ to 1 with stable chlorine isotopes (Zreda et al. 1991, Sheppard & Herod 2012). This corresponds to a concentration of approximately 1 Bq/(kg Cl).

^{36}Cl is also produced in the atmosphere by spallation of ^{36}Ar by interactions with cosmic ray protons. In the top meter of the lithosphere, ^{36}Cl is generated primarily by thermal neutron activation of ^{35}Cl and spallation of ^{39}K and ^{40}Ca (Zreda et al. 1991).

^{36}Cl decays in one step to stable isotopes, mainly by beta minus decay (β-, 98.1 %) to ^{36}Ar, and sometimes by electron capture/beta plus decay (ec/β+, 1.9 %) to ^{36}S. Hence, the decay products are mainly the noble gas argon and some sulphur.

In Swiss radioactive waste, more than 60 % of the ^{36}Cl activity is found in spent nuclear fuel where traces of ^{35}Cl in the fuel itself have been activated during operation in the reactor (Fig. 4, Tab. 3), where lots of thermal neutrons are available.

No ^{36}Cl is left in vitrified high-level waste from reprocessing. The volatile chlorine has evaporated during the reprocessing steps of the dissolved spent fuel; it is found in the surroundings of reprocessing plants (Calmet et al. 2001). However, other reprocessing wastes (hulls and ends, slurries etc.) still contain the original ^{36}Cl load, about 10 % of the total ^{36}Cl inventory (as ILW wastes, Fig. 4, Tab. 3).

^{36}Cl in low-level wastes (L/ILW) is mainly found in stainless reactor steel (85 %) and other metals (10 %) (Fig. 4).

In contrast to other nuclides discussed here, ^{36}Cl is distributed over many waste sorts, "a little bit everywhere". This is of course a direct consequence of the fact that wherever we have trace concentrations of stable Cl and a sufficient flux of thermal neutrons ^{36}Cl will be formed by neutron activation.

Nothing is known about the chemical form of ^{36}Cl any of these waste forms.

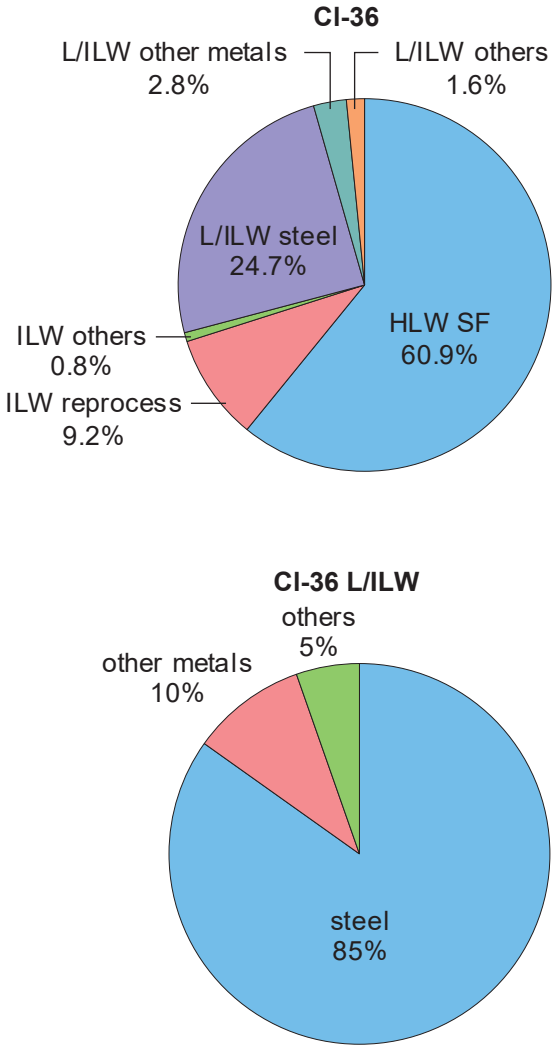

Fig. 4: Distribution of ^{36}Cl to different waste forms in mole percent according to MIRAM 14 (Nagra 2014b). Top: Total of all waste forms. Bottom: Low- and intermediate-level waste only.

The abbreviations are HLW: **H**igh-**L**evel **W**aste. SF: **S**pent nuclear **F**uel assemblies. ILW: long-lived **I**ntermediate-**L**evel **W**aste. reprocess: ILW from reprocessing (compacted hulls and ends, vitrified sludges). L/ILW: **L**ow- and **I**ntermediate-**L**evel **W**aste. steel: decommissioning waste, stainless steel from reactor internals.

Tab. 3: Distribution of ^{36}Cl to different waste forms according to MIRAM 14 (Nagra 2014b). Original data in [Bq], converted to [mol] assuming T½ = 3.013×10^5 years, converted to [Sv] using 9.3×10^{-10} [Sv/Bq].

The abbreviations are HLW: **H**igh-**L**evel **W**aste. SF: **S**pent nuclear **F**uel assemblies. ILW: long-lived **I**ntermediate-**L**evel **W**aste. reprocess: ILW from reprocessing (compacted hulls and ends, vitrified sludges). L/ILW: **L**ow- and **I**ntermediate-**L**evel **W**aste. steel: decommissioning waste, stainless steel from reactor internals.

The waste form codes are taken from Nagra (2014a, Tab. A3.1-7).

		[mol]	[Bq]	[Sv]
All waste types		145.57	6.42×10^{12}	5.97×10^3
HLW total	60.87 %	88.60	3.91×10^{12}	3.63×10^3
HLW SF BE-L-UO2-U-HAA BE-G-UO2-U-HAA BE-B-UO2-U-HAA BE-M-UO2-U-HAA BE-G-MOX-U-HAA BE-B-MOX-U-HAA	**60.87 %**	**88.60**	3.91×10^{12}	3.63×10^3
ILW total	10.01 %	14.57	6.42×10^{11}	597
ILW reprocess WA-F-MX-K1-ATA WA-F-SG-K1-ATA	**9.23 %**	**13.43**	5.92×10^{11}	551
ILW others	0.78 %	1.14	5.02×10^{10}	46
L/ILW total	29.12 %	42.4	1.87×10^{12}	1.74×10^3
L/ILW steel SA-B-ME-M2-SMA SA-G-ME-M2-SMA SA-M-ME-M2-SMA SA-L-ME-M2-SMA	**24.71 %**	**35.97**	1.59×10^{12}	1.47×10^3
L/ILW other metals	2.85 %	4.15	1.83×10^{11}	170
L/ILW others	1.56 %	2.27	1.00×10^{11}	93
Total	94.81 %			

2.2 Aqueous species and pure solid phases

Aqueous species

Chlorine occurs in aqueous solutions of environmental concern mainly as chloride, Cl^-, the thermodynamically stable form of chlorine in water.

Dissolved chlorine, $Cl_2(aq)$, and most oxidised forms of chlorine like hypochloride, ClO^-, chlorite, ClO_2^-, and chlorate, ClO_3^-, are highly reactive and are quickly reduced to chloride.

Dissolved chlorine disproportionates in pure water to hydrochloric acid, HCl, and hypochlorous acid, HClO. In alkaline solutions chloride and hypochloride is formed. Hypochloride is a strong oxidising agent, used for bleaching and disinfection. For example, calcium hypochloride, $Ca(ClO)_2$, is commonly used as bleaching powder and swimming pool "chlorine".

Chlorous acid, $HClO_2$, is the least stable oxoacid of chlorine, and sodium chlorite, $NaClO_2$, is used as a disinfectant.

Chlorates are powerful oxidizers and were once widely used in pyrotechnics, though their use has fallen due to their instability. Recently, natural chlorate has been discovered in the Atacama Desert (Rao et al. 2010).

The only fairly stable form of oxidised chlorine in aqueous solutions is perchlorate, ClO_4^-. $NaClO_4$ was widely used as an inert background electrolyte in experimental chemical thermodynamics in order to determine stability constants of metal – ligand complexes. Due to its relative stability, perchlorate can occur as a contaminant in drinking water.

The original chemical form of ^{36}Cl in radioactive waste forms is unknown. However, in the long run and especially under reducing conditions, which are expected in corroding spent nuclear fuel canisters and stainless reactor steel and other metal wastes, all these oxidised forms of chlorine, including perchlorate, if present at all, will be reduced to chloride.

Thus, in the following only the chemical thermodynamics of Cl^- will be discussed.

The interaction of chloride, Cl^-, with most cations is weak. Specifically, the interaction of Cl^- with all "hard" cations, including lanthanides and actinides, is described in thermodynamic models as weak complexation and/or specific ion interaction. The probably never ending discussion of experts in chemical thermodynamics about the most appropriate models concerning weak complexation versus specific ion interaction is of little practical importance in safety assessments.

However, Cl^- forms strong complexes with "soft" metal cations like Ag, Cd, Cu, Hg, Pb, Pd and Pt. In the acidic and neutral pH region, the speciation of these metal cations can be dominated by chloride complexes. In the alkaline, high pH region chloride complexation is only important at high to very high Cl^- concentrations (hydrolysis "wins") for almost all of the above mentioned elements with the only exception of Ag (very weak hydrolysis).

Chloride complexation can increase the solubility of these elements. By contrast, these metal compounds cannot act as "sinks" or solubility limiting phases for chloride due to their generally low concentrations compared with the concentrations of chloride in pore waters. For example, the reference pore water for Opalinus Clay contains 0.16 mol/L chloride (Mäder 2009). This is orders of magnitude higher than any expected concentration of the mentioned heavy metals.

Solid phases

Chloride forms highly soluble salts with all major and minor components of ground and surface waters; all alkali and alkaline earth elements, iron, manganese, nickel, copper, aluminium. These salts are only important if rock salt is considered as host rock of a geological repository.

The only sparingly soluble phases, also known as naturally occurring minerals, are AgCl (chlorargyrite) and Hg_2Cl_2 (calomel). Other pure phases formed with "soft" metal cations like $HgCl_2$ or $PbCl_2$ are soluble in the gram per litre range.

2.3 Surface interactions and solid solutions

Clay systems

In the case of spent fuel, the anion Cl^- will not sorb on clay minerals due to electrostatic repulsion from the negatively charged clay mineral surfaces, and it will not be incorporated in any solid phase of the bentonite backfill or the clay host rock.

Actually, chloride is used as "conservative tracer" in diffusion experiments with clay containing solids, as it is not retarded by any sorption or co-precipitation effects.

Cement systems

The uptake process of Cl^- in hardened cement paste (HCP) is still poorly understood in spite of new sorption measurements that have been published in the last years and novel information on the thermodynamics of Cl^- bearing minerals in cement paste (Wieland 2014).

The (low) R_d value of ^{36}Cl was found to decrease with increasing concentration of stable Cl^- in solution. The partitioning of stable Cl^- between HCP and solution in the different stages of the cement degradation seems to be a key factor influencing the extent of ^{36}Cl uptake by HCP. This suggests that ^{36}Cl binding occurs via an isotopic exchange process while the concentration of stable Cl^- in HCP is controlled by the formation of a solid solution (Wieland 2014).

In CO_3^{2-} containing cements, such as the HTS cement used for the solidification of radioactive waste in Switzerland, chloride binding by AFm phases predominantly occurs due to the formation of a solid solution between calcium monocarboaluminate, $3CaO \cdot Al_2O_3 \cdot CaCO_3 \cdot 11\ H_2O$, and Friedel's salt, $3CaO \cdot Al_2O_3 \cdot CaCl_2 \cdot 10\ H_2O$. Complete conversion of AFm phases (e.g. calcium monocarboaluminate, calcium monosulphoaluminate) to Friedel's salt may take place over time in the case of ingress of saline groundwater (Wieland 2014). However, saline groundwater also increases the isotopic dilution of ^{36}Cl.

Chemisorption was considered to control Cl^- retention by C-S-H phases. At C/S ratios > 1.2 the C-S-H surface is positively charged. This is the case in fresh cement paste in stage I and paste degraded to stage II of the cement degradation. The proportion of Cl^- bound per unit mass of solid material was found to be lower for C-S-H phases than for Friedel's salt (Wieland 2014).

A recent study published by Van Es et al. (2015) claims to have demonstrated ^{36}Cl retention by a cementitious backfill. However, not even qualitative conclusions can be drawn from this study, as discussed in the Appendix.

2.4 Potential changes in dose-rates

Considering the chemical behaviour of the chloride anion in clay pore waters, acting as a "conservative tracer", the large isotopic dilution of ^{36}Cl by stable ^{35}Cl and ^{37}Cl in the near and far field of a deep geological repository, and the long half-life of ^{36}Cl, no significant retardation effects are expected for ^{36}Cl.

However, it might be worthwhile to have a closer look at the source term.

^{36}Cl is the only dose-relevant radionuclide discussed here whose calculated inventory is solely based on measured or merely assumed trace concentrations of its stable isotopes which are impurities in nuclear fuel and structural reactor material.

It seems that the only measurements of stable chlorine and ^{36}Cl in nuclear fuel have been published by Tait et al. (1997). They found that the total average Cl impurity level of four un-irradiated CANDU UO_2 fuel samples was 2.3 ± 1.1 ppm, which is less than the 5 ppm initial Cl impurity concentration assumed in the first safety assessment calculation for ^{36}Cl (Sheppard et al. 1996). The latter value can be found in recent publications, e.g. Pipon et al. (2007): "Pristine chlorine … is present as an impurity in the nuclear fuel (< 5 ppm)."

The cladding also contains traces of stable chlorine. The only measurements published are for Zr-2.5Nb pressure tubes for CANDU reactors: Aitchison & Davies (1993) found Cl impurities between 1 – 5 ppm.

Stainless steel is used extensively in nuclear reactors as a construction material and may be exposed to high neutron fluxes. Robertson et al. (2000) report that stainless steel Type 304 used in reactor internal hardware has Cl concentrations ranging from less-than 50 to 130 ppm Cl. Actually these values have been published originally by Evans et al. (1984, Tab. 4.8) based on five measurements of different samples where only one measurement was above the detection limit of Cl. Hou et al. (2007) state: "No report on the analysis of steel for ^{36}Cl is available".

Spent fuel (HLW SF) is calculated to contain 61 % of the total ^{36}Cl activity, and stainless steel from reactor decommissioning (L/ILW steel) 25 % total (or 85 % of the L/ILW) activity (Fig. 4). These calculated concentrations of activated ^{36}Cl might be overestimated by orders of magnitude because they depend on very few measurements and many (pessimistic) assumptions about ^{35}Cl trace concentrations.

2.5 Conclusions and further research topics

No significant retardation effects are expected for ^{36}Cl. It seems also improbable that hitherto major chemical solubility and retardation phenomena have been overlooked.

By contrast, a more detailed determination of ^{36}Cl in spent fuel, cladding and stainless steel seems to be the most promising future research topic with the potential to significantly reduce the ^{36}Cl inventory and thus the calculated dose-rates of ^{36}Cl.

3 Se-79

3.1 Origin and initial waste forms

Selenium has six stable isotopes, ^{74}Se (0.89 %), ^{76}Se (9.37 %), ^{77}Se (7.63 %), ^{78}Se (23.77 %), ^{80}Se (49.61 %) and ^{82}Se (8.73 %), one long-lived radioactive isotope, ^{79}Se, with a half-life of $(3.27 \pm 0.08) \cdot 10^5$ years, and two short-lived radioactive isotopes (^{75}Se: 119.78 days, ^{72}Se: 8.5 days). All other radioactive selenium isotopes have half-lives less than eight hours.

All of the above mentioned stable selenium isotopes and the long-lived radioactive isotope, ^{79}Se, are produced in the course of ^{235}U and ^{239}Pu fission by thermal neutrons in nuclear reactors. The cumulative fission yield of ^{79}Se is 0.0487 % and 0.0550 % for ^{235}U and ^{239}Pu fission, respectively. The sums of cumulative fission yields for all stable selenium isotopes, Se(stable), are 0.485 % (^{235}U fission) and 0.3639 % (^{239}Pu fission). Hence, the "intrinsic" isotopic dilution factor ^{79}Se/Se(stable) is 0.10 and 0.15 for ^{235}U and ^{239}Pu fission, respectively.

In addition, in a nuclear reactor ^{75}Se and ^{79}Se are produced by neutron capture of the stable nuclides ^{74}Se and ^{78}Se, respectively. The reaction $^{74}\text{Se} + {}^{1}\text{n} \rightarrow {}^{75}\text{Se} + \gamma$ has a high cross section of 51.77 barn, whereas the reaction $^{78}\text{Se} + {}^{1}\text{n} \rightarrow {}^{79}\text{Se} + \gamma$ has a small cross section of 0.4005 barn.

^{74}Se has a high cross section, but its natural abundance is the lowest of all stable selenium isotopes (0.89 %) and the activation product ^{75}Se has a half-life of 119.6 days only. So, whatever small amount of short-lived ^{75}Se is produced by neutron activation, it decays in interim storage and is completely gone after less than 10 years of storage.

On the other hand, although ^{78}Se has a small cross section, it constitutes about one quarter of natural selenium and its activation product ^{79}Se is very long-lived. So, even trace amounts of ^{78}Se in structural material are sufficient to produce significant amounts of ^{79}Se provided that we have a sufficient flux of thermal neutrons.

^{79}Se decays by simple beta minus decay (β-) to stable ^{79}Br, a halogen element which is not expected to significantly interfere with any chemical processes going on in and around a geological repository.

In Swiss radioactive waste, 99.5 % of the total ^{79}Se activity is found in spent nuclear fuel and vitrified high-level waste from reprocessing (Fig. 5). The non-volatile fission product ^{79}Se in spent fuel is not separated during reprocessing, in contrast to the volatile elements Cl and I, and completely remains in the residual liquid high-level waste, which is then vitrified. The observation that we find about equal fractions of ^{79}Se activity in spent nuclear fuel and vitrified high-level waste is by coincidence. Originally, all spent fuel was sent to reprocessing facilities, and vitrified high-level waste had to be taken back, but 10-year moratorium on reprocessing lead to increasing amounts of spent fuel for direct disposal. The estimated activity distribution between the two waste forms now depends on the life-time of Swiss nuclear power plants. However, the total amount of ^{79}Se to be disposed of will remain the same.

^{79}Se in low-level wastes (L/ILW) is mainly found in stainless reactor steel (97 %) (Fig. 5). This ^{79}Se is a neutron activation product of trace amounts of selenium in reactor steel.

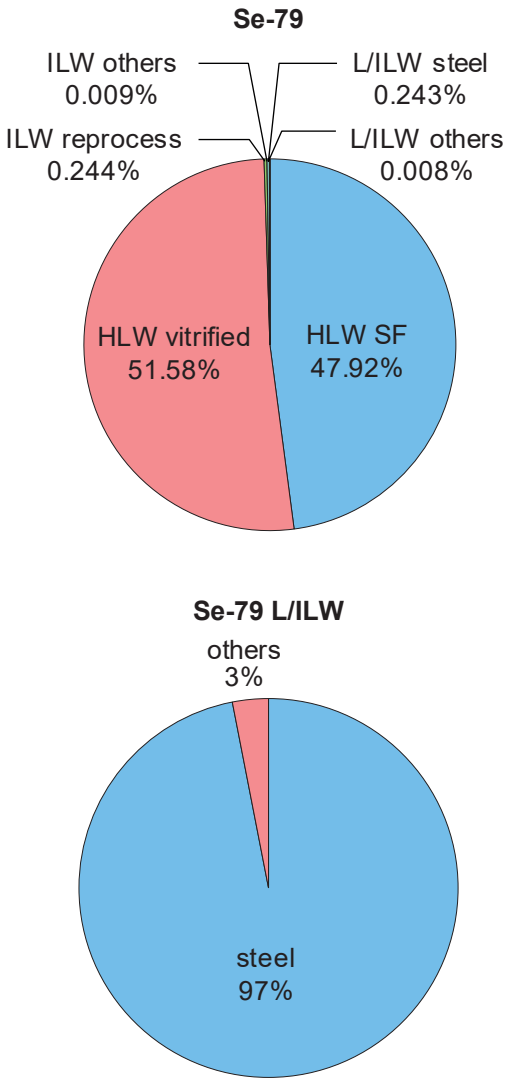

Fig. 5: Distribution of ^{79}Se to different waste forms in mole percent according to MIRAM 14 (Nagra 2014b). Top: Total of all waste forms. Bottom: Low- and intermediate-level waste only.

The abbreviations are HLW: **H**igh-**L**evel **W**aste. SF: **S**pent nuclear **F**uel assemblies. HLW vitrified: vitrified HLW from reprocessing of spent fuel. ILW: long-lived **I**ntermediate-**L**evel **W**aste. reprocess: ILW from reprocessing (compacted hulls and ends, vitrified sludges). L/ILW: **L**ow- and **I**ntermediate-**L**evel **W**aste. steel: decommissioning waste, stainless steel from reactor internals.

Tab. 4: Distribution of ^{79}Se to different waste forms according to MIRAM 14 (Nagra 2014b). Original data in [Bq], converted to [mol] assuming $T½ = 3.27 \times 10^5$ years, converted to [Sv] using 2.9×10^{-9} [Sv/Bq].

The abbreviations are HLW: **H**igh-**L**evel **W**aste. SF: **S**pent nuclear **F**uel assemblies. HLW vitrified: vitrified HLW from reprocessing of spent fuel. ILW: long-lived **I**ntermediate-**L**evel **W**aste. reprocess: ILW from reprocessing (compacted hulls and ends, vitrified sludges). L/ILW: **L**ow- and **I**ntermediate-**L**evel **W**aste. steel: decommissioning waste, stainless steel from reactor internals.

The waste form codes are taken from Nagra (2014a, Tab. A3.1-7).

		[mol]	[Bq]	[Sv]
All waste types		579.1	2.34×10^{13}	6.79×10^4
HLW total	99.50 %	576.18	2.33×10^{13}	6.76×10^4
HWL SF BE-L-UO2-U-HAA BE-G-UO2-U-HAA BE-B-UO2-U-HAA BE-M-UO2-U-HAA BE-G-MOX-U-HAA BE-B-MOX-U-HAA	**47.92 %**	**277.50**	1.12×10^{13}	3.26×10^4
HLW vitrified WA-F-KG-K1-HAA WA-U-KG-K1-HAA	**51.58 %**	**298.68**	1.21×10^{13}	3.50×10^4
ILW total	0.253 %	1.46	5.92×10^{10}	172
ILW reprocess WA-F-MX-K1-ATA WA-F-SG-K1-ATA	0.244 %	1.41	5.71×10^{10}	166
ILW others	0.009 %	0.05	2.05×10^9	6
L/ILW total	0.251 %	1.46	5.89×10^{10}	171
L/ILW steel SA-B-ME-M2-SMA SA-G-ME-M2-SMA SA-M-ME-M2-SMA SA-L-ME-M2-SMA	0.243 %	1.41	5.69×10^{10}	165
L/ILW others	0.008 %	0.05	1.99×10^9	6

The chemical state of ^{79}Se in spent nuclear fuel (SF) has recently been investigated within the scope of the EU-funded project "FIRST-Nuclides". The major results are (Curti et al. 2014; Curti et al. 2015):

A micro X-ray fluorescence study on samples from Gösgen/Leibstadt showed that Se is present in substantial amounts in all SF samples and it is homogeneously distributed (i.e. no "hot spots"). Micro-X-ray Absorption Near Edge Structure (Micro-XANES) ‘fingerprinting' indicates Se(-II) as primary redox state in UO_2 SF from two boiling water reactors. XANES and Extended X-Ray Absorption Fine Structure (EXAFS) calculated spectra are consistent with substitution of Se(-II) for O(-II) in the expanded UO_2 lattice (Fig. 6).

In this form, selenium is almost insoluble and can be released only very slowly via UO_2 matrix dissolution. Thus, the spectroscopic data explain the unexpectedly low release of Se found in leach experiments within the "FIRST-Nuclides" project.

This result is highly plausible considering that ^{79}Se is a fission product of ^{235}U, actually "created" within the UO_2 fuel matrix and subsequently incorporated in the UO_2 crystal lattice by replacing O^{2-} as Se^{2-}.

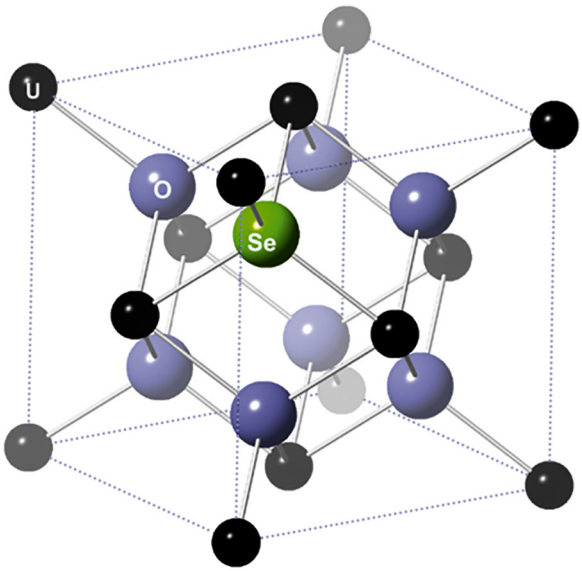

Fig. 6: Substitution of Se(-II) for O(-II) in the expanded UO_2 lattice.
Figure provided by Enzo Curti.

The chemical state of ^{79}Se in vitrified high-level waste (HLW) also has been elucidated by XANES spectroscopy (Curti et al. 2013). As shown in Fig. 7, selenium in vitrified radioactive waste simulate occurs as Se(IV), i.e. as SeO_3^{2-}. This result has been confirmed by Dardenne et al. (2015) by XANES spectra of an actual radioactive HLW glass fragment obtained from the Karlsruhe vitrification plant. Again, this result is highly plausible, as both the hot nitric acid dissolution of the spent fuel and the vitrification process of the highly radioactive reprocessing residues are oxidising processes, and selenium originally present as Se^{2-} in the UO_2 fuel matrix is oxidised in these processes.

Nothing is known about the chemical state of ^{79}Se in stainless reactor steel.

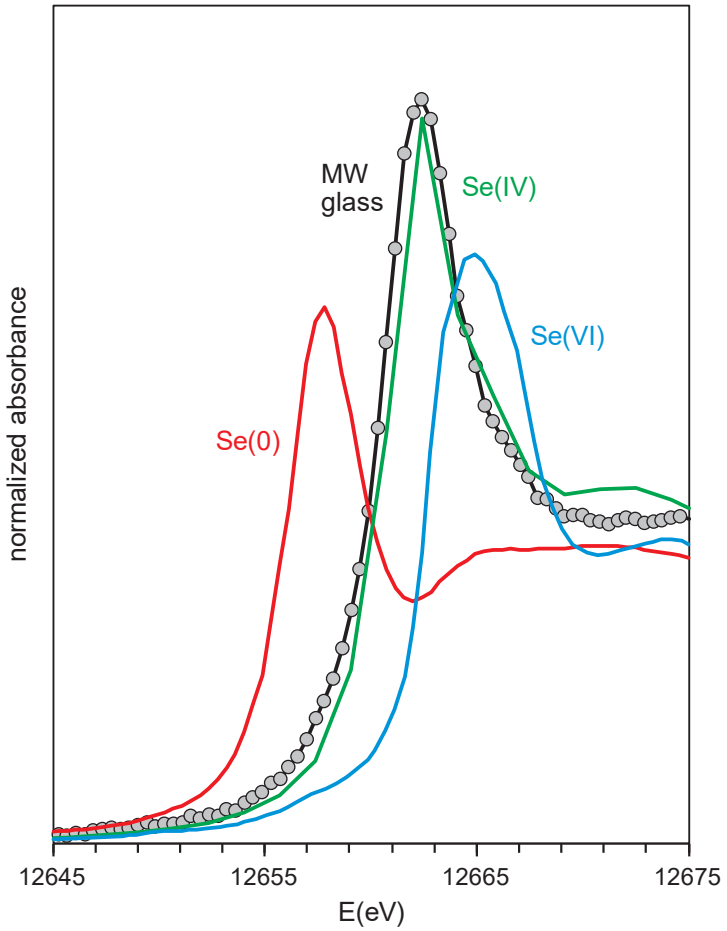

Fig. 7: XANES spectrum of a vitrified radioactive waste simulate (MW), compared to the spectra of reference compounds for Se(0), Se(IV) and Se(VI).

Figure provided by Enzo Curti, modified after Curti et al. (2013).

3.2 Aqueous species and pure solid phases

Aqueous species

A comprehensive review of published experimental data on the chemical thermodynamics of selenium has been published in 2005 by NEA (Olin et al. 2005). The recommended values selected in this review are now widely used in thermodynamic calculations involving selenium species. The values are of high quality, probably the best data available today.

Speciation of selenium in aqueous solution is complicated by the fact that selenium is a redox sensitive element with four stable redox states in water: Se(-II), Se(0), Se(IV) and Se(VI). Most selenium species in "pure" water are negatively charged ions, in the case of Se(IV) and Se(VI) oxo-anions, and only in the acidic region some charge neutral acids predominate (Fig. 8).

All these anions can form complexes with metal cations. The complexes with major groundwater constituents like Na^+, K^+, Mg^{2+}, Ca^{2+} and Sr^{2+} are weak or can be described by specific ion

interactions only. Some cases of strong complexes are known, e.g. $FeSeO_3^+$. An exhaustive review of all available experimental complexation data is given by Olin et al. (2005).

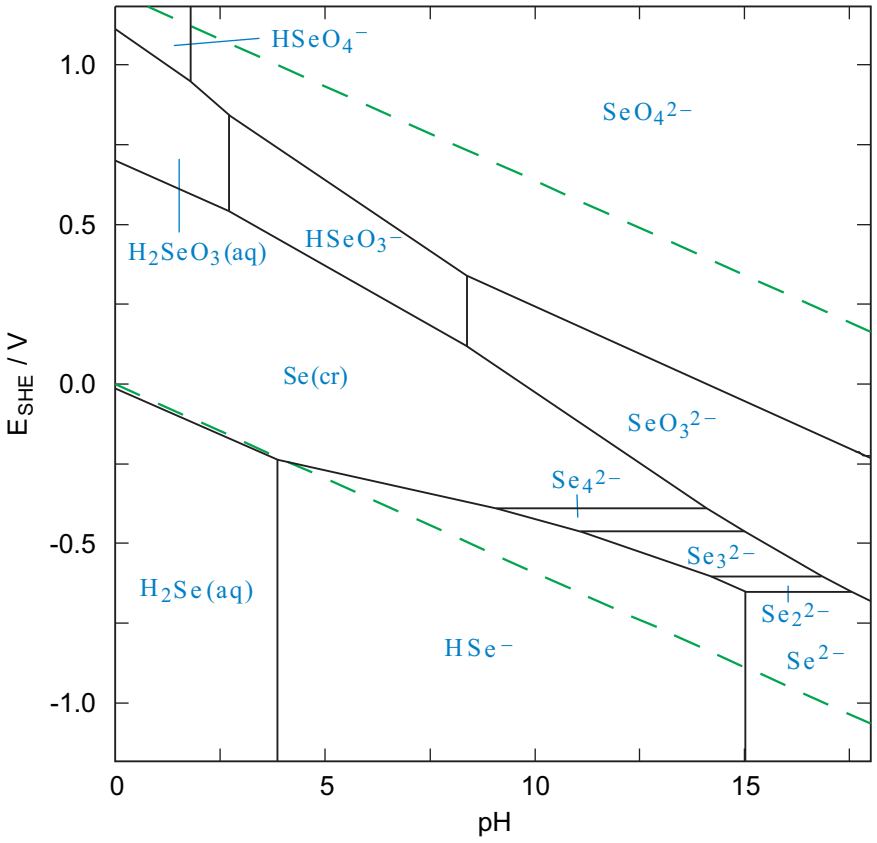

Fig. 8: Predominance diagram of selenium species in "pure" water as a function of pH and redox conditions (E_{SHE} refers to the standard hydrogen electrode, in volts), $[Se]_{total}$ = 10^{-3} mol dm^{-3}, T = 25°C.

The dashed lines indicate the stability limits of water. Thermodynamic data taken from Olin et al. (2005).

So far, the basic chemical thermodynamics of selenium seems to be settled. However, when doing solubility calculations involving selenium strange results are obtained. In "pure" water at pH 7 and varying Eh conditions the solubility of selenium drops to values below 10^{-15} mol dm^{-3} close to Eh = 0 V (Fig. 9). At pH < 7 we may reach values as low as 10^{-18} mol dm^{-3}. The edges of this "solubility abyss" are dominated by the selenide species HSe^- at Eh < 0 and by the selenite species $HSeO_3^-$ at Eh > 0 (Fig. 9). This result is not new, it has puzzled modellers in the past, but the reason remained unclear. The solution of this enigma starts with the question: Why is there no dissolved selenium in redox state zero, i.e. Se(aq), in the thermodynamic database which would remove this unreasonable "solubility abyss" (question mark in Fig. 9)?

In the chemically similar sulphur system the existence of dissolved sulphur in redox state zero is well established and several experimental studies have been published (Boulege 1978, Kamyshny 2009, Wang & Tessier 2009) resulting in a value of S(aq) = 2×10^{-7} mol dm^{-3} in the presence of elemental sulphur, S(cr). In the selenium system, the equilibrium of elemental selenium, Se(cr), with respect to selenide, $Se(cr) + 2\ e^- \rightleftharpoons Se^{2-}$, is given as a "selected value" by Olin et al. (2005) but the possible existence of Se(aq) is not even mentioned.

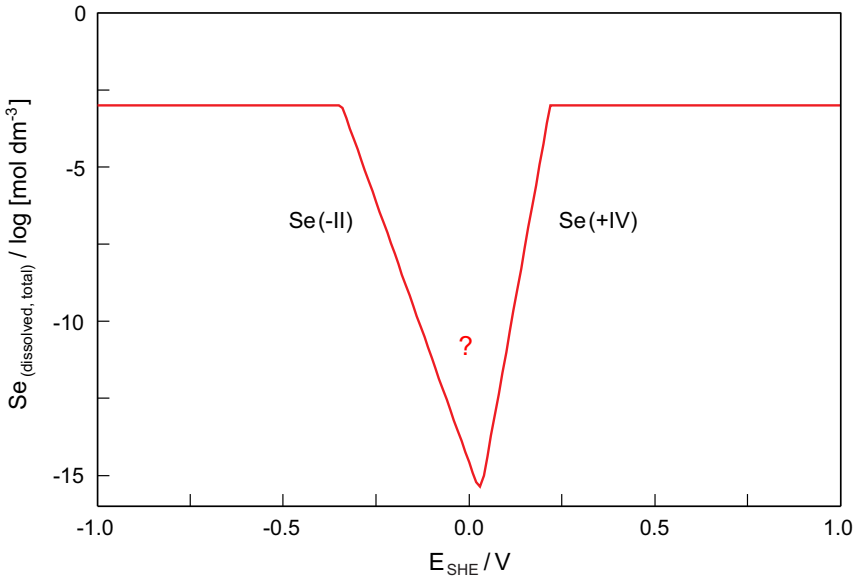

Fig. 9: Solubility of selenium in "pure" water at pH = 7.0, $[Se]_{total} = 10^{-3}$ mol dm^{-3}, T = 25°C and varying redox conditions (E_{SHE} refers to the standard hydrogen electrode, in volts).

Thermodynamic data taken from Olin et al. (2005).

A closer look at the experimental conditions of the crucial data sets used by Olin et al. (2005) to derive the solubility of Se(cr) resolves the enigma of missing Se(aq) data: The experiments involving Se(cr) either aimed at determining the Se(0)/Se(IV) redox potential at very low pH or elucidated the redox potentials of the polyselenides $Se_2^{2-}/Se_3^{2-}/Se_4^{2-}$ at very high pH (Fig.10).

Hence, the solubility of Se(cr) has been determined in the presence of selenous acid, H_2SeO_3(aq), at pH < 2, or in the presence of polyselenides at pH > 13 (Fig. 10). The actual solubility of Se(cr) in near-neutral solutions and the possible presence of Se(aq) was, and still is "terra incognita" (question mark in Fig. 10).

The extreme pH conditions of the polyselenide redox studies (Fig. 10) may also be the reason why the tetraselenide, Se_4^{2-}, is the longest selenium polymer identified so far, while in the sulphur system polysulphides up to S_8^{2-} have been found (Kamyshny et al. 2004). Dedicated studies at lower pH might reveal the existence of longer selenium polymers.

Recently, Iida et al. (2010) measured the solubility of selenium in this "terra incognita", 5 < pH < 13. Above pH 9 their results are consistent with the dataset of Olin et al. (2005). Below pH 9 they measured higher total selenium concentrations than predicted with the dataset of Olin et al. (2005), and they postulated a phase transition from Se(cr) to an amorphous selenium phase below pH 9, although they found Se(cr) by X-ray powder diffraction (XRD) in all cases. Identification of Se(cr) by XRD does not exclude the presence of an amorphous selenium layer on the surface of Se(cr) or of un-crystallised solid but there is no independent evidence that such a layer or un-crystallised solid should exist solely below pH 9. Hence, a re-interpretation of the experimental data by the present author (see Appendix) suggests that Iida et al. (2010) actually measured the protonation of a polyselenide, presumably $Se_4^{2-} + H^+ \rightleftharpoons HSe_4^-$. Furthermore, their data indicate an upper limit for the solubility of Se(cr) $\rightleftharpoons$ Se(aq) of Se(aq) < 10^{-5} mol dm^{-3}. However, all these results need confirmation.

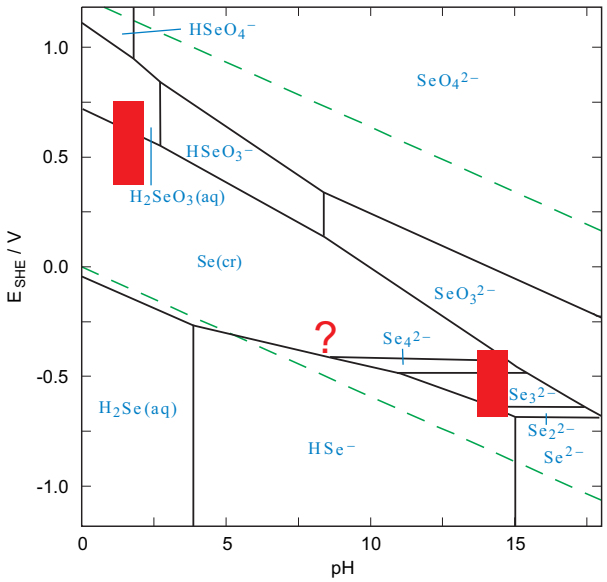

$Se(cr) + 2I_2(cr) + 3H_2O(l)$

⇔

$H_2SeO_3(aq) + 4H^+ + 4I^-$

0.01 – 0.05 M $HClO_4$

Redox potentials

½ Se_2^{2-} / Se^{2-}

1/3 Se_3^{2-} / Se^{2-}

¼ Se_4^{2-} / Se^{2-}

0.5 – 2 M KOH

H.F. Schott, E.H. Swift, D.M. Yost, *J. Am. Chem. Soc.* **50** (1928) 721-727.

L.E. Lyons, T.L. Young, *Aust. J. Chem.* **39** (1986) 511-527.

S. Licht, F. Forouzan, *J. Electrochem. Soc.* **142** (1995) 1546-1551.

Fig. 10: Predominance diagram of selenium in "pure" water at $[Se]_{total} = 10^{-2}$ mol dm^{-3} and T = 25°C.

Thermodynamic data taken from Olin et al. (2005).

In summary, the speciation of the selenium – water system is incomplete, especially in near-neutral conditions. The species Se(aq), dissolved selenium in redox state zero, has not been considered in any study, and the lowest attainable solubility of Se(cr) in near-neutral solutions is unknown. Besides Se(aq), selenium polymers longer than the tetramer might exist in these solutions, and their polymerisation equilibria and the protonation constants of these polymers need to be determined.

Solid phases

Thermodynamic data for a large number of selenium solids have been reviewed by Olin et al. (2005). They recommend thermodynamic equilibrium data derived from solubility measurements for many metal – selenate solids, which are generally highly soluble, and also for many metal – selenite solids, which are less soluble, but no such data are available for metal – selenide solids.

All thermodynamic data recommended by Olin et al. (2005) for metal – selenide solids were derived from calorimetric measurements of solids which "have never seen" an aqueous solution. Although the heat capacity measurements in these cases are very accurate and the solids well characterised, solubilities calculated using these data are wrong by orders of magnitude, as no information about the corresponding aqueous metal – selenide complexes is available.

For example, the Gibbs free energy value recommended by Olin et al. (2005) for $FeSe_2$(cr) is derived from several (consistent) heat capacity measurements in the temperature range 5 to 853 K, in combination with the measured enthalpy of decomposition of $FeSe_2$(cr) into γ-Fe_3Se_4 and liquid selenium. No information at all is available concerning aqueous Fe(II) – selenide complexes. Hence, the solubility of $FeSe_2$(cr) in water is unknown and cannot be calculated from existing thermodynamic data.

3.3 Surface interactions and solid solutions

Cement systems

Strong uptake of Se(VI) was observed by ettringite, $Ca_6Al_2(SO_4)_3(OH)_{12}\cdot 26H_2O$ or $3CaO\cdot Al_2O_3\cdot 3CaSO_4\cdot 32H_2O$, and hardened cement paste (HCP) under conditions where secondary ettringite formed. In contrast, Se(VI) uptake by primary ettringite which forms in the early stage of cement hydration was much weaker and calcium monosulphoaluminate, $3CaO\cdot Al_2O_3\cdot CaSO_4\cdot 11H_2O$, was observed to strongly bind Se(VI). These observations suggest that ettringite and/or calcium monosulphoaluminate may be responsible for SeO_4^{2-} binding to HCP. Ochs et al. (2002) developed a simplified solid solution model on Se(VI) – ettringite interaction which resulted in an empirical relationship between SeO_4^{2-} uptake by HCP and the SO_4^{2-} concentration in solution (Wieland 2014).

Uptake of SeO_3^{2-} by HCP was found to be less specific with respect to the mineral phase involved. LES in-house measurements with SeO_3^{2-} on ettringite, AFm phases and C-S-H phases support the findings from an earlier study. It is anticipated that SeO_3^{2-} retention in HCP occurs predominantly due to the replacement of SO_4^{2-} by SeO_3^{2-} in ettringite or calcium monosulphoaluminate in the first two stages of the cement degradation (Wieland 2014).

The retention of Se(0) and Se(-II) in HCP is not discussed by Wieland (2014) as no relevant sorption data are presently available. This lack of data is unfortunate because 97 % of the ^{79}Se activity in L/ILW waste is estimated to be decommissioning waste in form of stainless steel from reactor internals (Fig.5). The chemical form of ^{79}Se in this stainless steel is unknown, but whatever redox state these trace amounts of Se in the metallic iron matrix are, by corrosion of Fe(0) we expect Se(0) and/or Se(-II) as corrosion product. Experimental and modelling work within the scope of the ongoing CEBAMA project, http://www.cebama.eu/, aims at remedying this situation with respect to the ion-exchange behaviour of Se(-II) onto relevant AFm phases.

Clay systems

No sorption data are available for Se(-II) in clay systems (Baeyens et al. 2014).

In a recent study using micro- and bulk X-ray spectroscopy (μ-XRF, μ-XANES and EXAFS) Curti et al. (2013) showed that, under nearly anoxic conditions, dissolved SeO_3^{2-} and SeO_4^{2-} sorb directly onto pyrite, FeS_2, surfaces and are subsequently reduced to Se(0) with increasing ageing time (up to 8 months). These observations were confirmed by experiments studying the interaction of selenite with reduced Fe and/or S species where the reaction products also were characterised by a combination of methods (SEM, XRD and XAS): Finck & Dardenne (2016) showed that upon interaction with mackinawite, FeS, Se(IV)aq was reduced to Se(0) and minute amounts of pyrite were detected, a consequence of partial mackinawite oxidation at surface sulphur sites.

These results show that after release of $^{79}Se(IV)$ from vitrified high-level waste, selenite can be reduced in the near field to low soluble Se(0) by interaction with Fe(II)aq and/or S(−II)aq species. Note that pyrite (1-3 wt%) and siderite ($FeCO_3$) (4-15wt%) is found in Opalinus Clay (Traber & Blaser 2013).

Diener & Neumann (2011) and Diener et al. (2012) investigated the uptake of Se(IV) and Se(-II) by sulphides synthesised in batch experiments under anoxic conditions. Results from X-ray diffraction and scanning electron microscopy analyses revealed the formation of pyrite, FeS_2, and mackinawite, FeS. More than 98 % of the Se added to solutions (initial concentration: 10^{-3} – 10^{-6} mol/L) was taken up by the Fe sulphide minerals. Focused beam analysis showed an inhomogeneous Se distribution with a higher accumulation in the centre of the pyrite grains, probably due to the progressive depletion of Se from solution with regard to S.

XAFS results (Diener et al. 2012) indicate a substitution of sulphur by selenide during instantaneous precipitation in highly supersaturated solutions only. In selenide doted mackinawite S^{2-} was substituted by Se^{2-}, resulting in a mackinawite-type compound. S^- is substituted by Se^- in selenide-doted pyrite, yielding a FeSSe compound as a slightly distorted pyrite structure. Under slightly supersaturated conditions, XAFS results indicate an incorporation of Se(-II) and Se(IV) predominantly as Se(0). This study shows that a substitution of S by Se in iron sulphides is probable only for highly supersaturated solutions under acidic and anoxic conditions. Under closer equilibrium conditions, Se(0) is expected to be the most stable species.

In a parallel study by Finck et al. (2012), the selenide retention by co-precipitation with and by adsorption on mackinawite, FeS, was investigated. XRD and SEM analyses of the samples reveal no significant influence of Se on the mackinawite precipitate morphology and structure. Samples from co-precipitation and from adsorption are characterized at the molecular scale by a multi-edge X-ray absorption spectroscopy (XAS) investigation. In the co-precipitation experiment, all elements (S, Fe, and Se) are in a low ionic oxidation state and the EXAFS data strongly point to selenium located in a mackinawite-like sulphide environment. By contacting selenide ions with FeS in suspension, part of Se is located in an environment similar to that found in the co-precipitation experiment. The explanation why Se in this latter experiment is not just found at the surface of the FeS particles in suspension but incorporated similar to the co-precipitation experiment is a dynamical dissolution−recrystallization mechanism of the highly reactive mackinawite.

These results imply that pyrite and its most important precursor phase, mackinawite, are efficient in removing selenium from solution by forming $FeSe_xS_y$ solid solutions. Probably Se(0) is incorporated or formed as a separate phase. However, no reliable solubility studies have been published so far and the effect of selenium removal from solution cannot be quantified yet.

3.4 Conclusions and further research topics

The chemical state of selenium in spent nuclear fuel (SF) has recently been clarified. Selenium Se(-II) replaces O(-II) in the UO_2 matrix , and its "instant release fraction", i.e. Se in cracks and gaps of the spent nuclear fuel rods is very small to perhaps inexistent. Hence, Se(-II) will be released from SF very slowly by dissolution of the UO_2 matrix. Considering the reducing environment due by UO_2 dissolution, and the additional redox effect by the corroding steel canister, we expect non-oxidised HSe^- in solution. The formation of oxidised Se(aq), although improbable, cannot be ruled out a priori as the thermodynamics of Se(aq) is not explored yet.

The chemical state of selenium in vitrified high-level waste (HLW) has also recently been clarified. Selenium occurs in the glass matrix as Se(IV) and will be released as SeO_3^{2-} or $HSeO_3^-$

by glass corrosion, depending on the pH of the pore water. Considering the redox effect of the corroding steel canister, we expect quick reduction to Se(aq) and probably further reduction to HSe^- can be expected.

^{79}Se in low-level waste (L/ILW) is mainly found in stainless reactor steel, created by neutron activation of traces of ^{78}Se in the steel. Nothing is known about the chemical state of ^{79}Se in reactor steel. However, corrosion of this waste form, essentially Fe(0), will create a strongly reducing environment and the released selenium is expected to be Se(aq) or HSe^-.

In summary, the chemical form of selenium released from the most important waste forms is expected to be very similar:

SF	(Se in UO_2 matrix + corroding steel canister)	$Fe(0) \rightarrow Fe^{2+}$, $Se(-II) \rightarrow HSe^-$ (Se(aq))
HLW	(Se in glass matrix + corroding steel canister)	$Fe(0) \rightarrow Fe^{2+}$, $Se(IV) \rightarrow Se(aq), HSe^-$
L/ILW	(Se in corroding reactor steel)	$Fe(0) \rightarrow Fe^{2+}$, $Se(?) \rightarrow Se(aq), HSe^-$

A potential sink for dissolved Se in the near-field is the formation of ferroselite, $FeSe_2$(cr). However, no information at all is available concerning aqueous Fe(II) – selenide complexes and thus, the solubility of $FeSe_2$(cr) in water cannot be calculated from existing thermodynamic data.

Recently it has been shown that pyrite, FeS_2(cr), and its most important precursor phase mackinawite, FeS(cr), are efficient in removing selenium from solution by forming $FeSe_xS_y$ solid solutions. Probably Se(0) is incorporated or formed as a separate phase. The formation of these solid solutions may lead to much lower selenium solubilities as the formation of the pure ferroselite, $FeSe_2$(cr). However, no reliable solubility studies have been published so far and the effect of selenium removal from solution by $FeSe_xS_y$ formation cannot be quantified yet.

In summary, the most promising research topics leading to a deeper understanding of aqueous selenium chemistry in reducing environments and most probably resulting in a lower selenium solubility than calculated so far with insufficient thermodynamic data are:

- Experimental and modelling studies of the system $Se(cr) \rightleftharpoons Se(aq)$, including the formation of polyselenides (HSe_x^-) and
- Experimental and modelling studies of the formation and solubility of $FeSe_2$(cr) and $FeSe_xS_y$ solid solutions

4 Ag-108m

4.1 Origin and initial waste forms

Silver has two stable isotopes, ^{107}Ag and ^{109}Ag, with natural abundances of 51.839 % and 48.161 %, respectively; one long-lived radioactive isotope, ^{108m}Ag, with a half-life of 437.7 ± 8.8 years, and two short-lived radioactive isotopes, ^{110m}Ag and ^{105}Ag with half-lives of 249.83 ± 0.04 and 41.29 ± 0.07 days, respectively. All other radioactive silver isotopes have half-lives less than nine days.

In a nuclear reactor ^{108m}Ag and ^{110m}Ag are produced by neutron capture of the stable nuclides ^{107}Ag and ^{109}Ag, respectively. The reaction $^{107}Ag + {}^{1}n \rightarrow {}^{108m}Ag + \gamma$ has a high cross section of 37.64 barn, whereas the reaction $^{109}Ag + {}^{1}n \rightarrow {}^{110m}Ag + \gamma$ has an even higher cross section of 90.81 barn. Thus, even trace amounts of stable silver in nuclear fuel and structural material are sufficient to produce ^{108m}Ag and ^{110m}Ag provided that we have a sufficient flux of thermal neutrons.

The short-lived ^{110m}Ag mainly decays in interim storage, and with its half-life of less than one year it is completely gone after 40 years of storage. Hence, only the long-lived ^{108m}Ag will be discussed further here.

The decay mode of ^{108m}Ag has several branches: The majority of ^{108m}Ag reacts via electron capture/beta plus decay (ec/β+ 91.3 %) to stable ^{108}Pd, while some ^{108m}Ag undergoes internal transition (IT 8.7 %) to ^{108}Ag which itself is radioactive with a half-life of 2.382 ± 0.011 minutes. The majority of ^{108}Ag reacts via beta minus decay (β- 97.15 %) to stable ^{108}Cd, and sometimes via electron capture/beta plus decay (ec/β+ 2.85 %) to stable ^{108}Pd. Hence, the stable decay products are the metals cadmium and palladium.

In Swiss radioactive waste, more than 98 % of the total ^{108m}Ag activity is found in a single waste form in the low-level waste category (Fig. 11). In the low-level wastes alone it contributes 99.7 % of the ^{108m}Ag activity. The waste form comprises activated control rods from pressurized water reactors. These control rods consist of an Ag-In-Cd alloy with about 80 % silver content. Hence, the waste form can be considered as metallic silver with some "impurities".

The ^{108m}Ag activity in ILW wastes is also completely dominated (95 %) by a single waste form (Fig. 11), control rods from the prototype reactor Lucens. These control rods consist of an Ag-Zr alloy. Again, this waste form can be considered as metallic silver with some "impurities".

The remaining small fraction of the total ^{108m}Ag activity (1.54 %) is attributed to activation products of trace amounts of silver in spent nuclear fuel, stainless reactor steel and other materials (Fig. 11).

In summary, the major source of ^{108m}Ag is metallic silver containing ^{108m}Ag as an activation product.

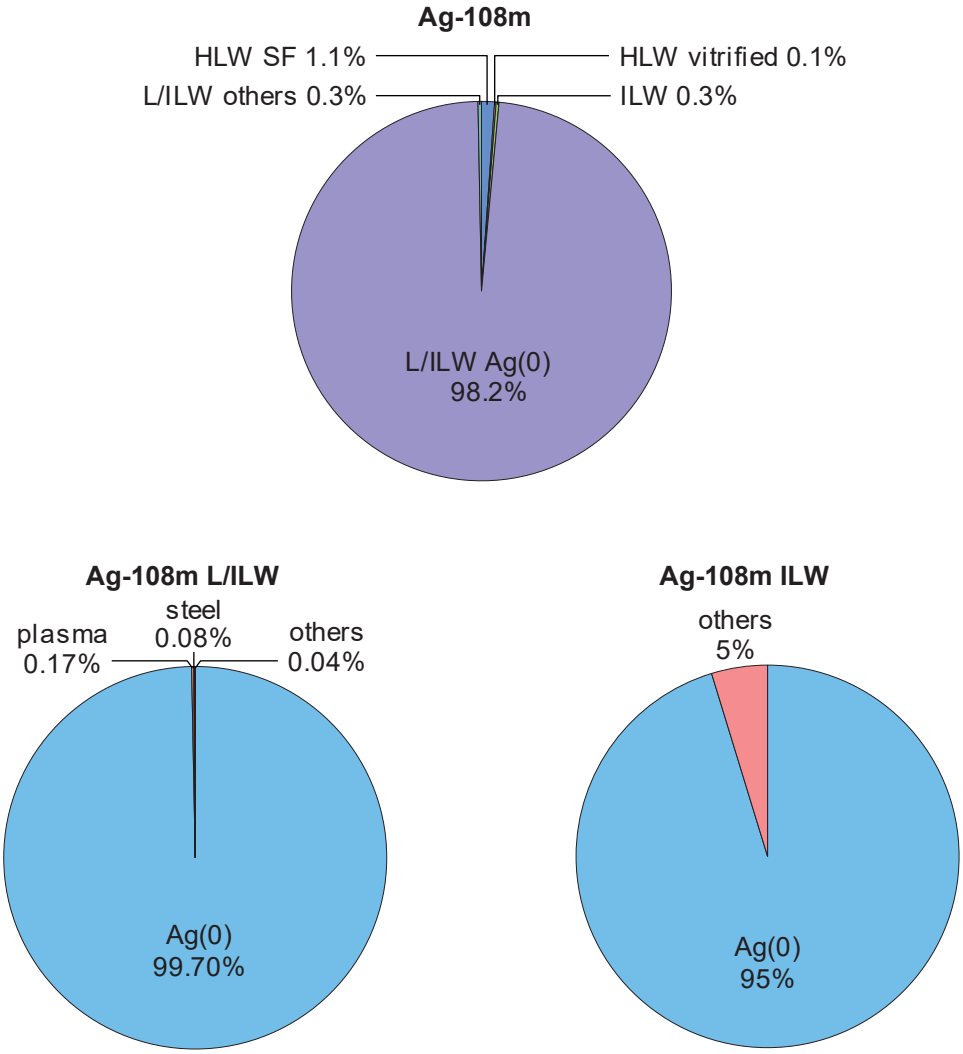

Fig. 11: Distribution of ^{108m}Ag to different waste forms in mole percent according to MIRAM 14 (Nagra 2014b). Top: Total of all waste forms. Bottom left: low- and intermediate-level waste only. Bottom right: long-lived intermediate-level waste only.

The abbreviations are HLW: **H**igh-**L**evel **W**aste. SF: **S**pent nuclear **F**uel assemblies. vitrified: vitrified HLW from reprocessing of spent fuel. ILW: long-lived **I**ntermediate-**L**evel **W**aste. L/ILW: **L**ow- and **I**ntermediate-**L**evel **W**aste. Ag(0): metallic silver. plasma: waste incinerated in the ZWILAG plasma plant. steel: decommissioning waste, stainless steel from reactor internals.

Tab. 5: Distribution of ^{108m}Ag to different waste forms according to MIRAM 14 (Nagra 2014b). Original data in [Bq], converted to [mol] assuming T½ = 418 years, converted to [Sv] using 2.3×10^{-9} [Sv/Bq].

The abbreviations are HLW: **H**igh-**L**evel **W**aste. SF: **S**pent nuclear **F**uel assemblies. vitrified: vitrified HLW from reprocessing of spent fuel. ILW: long-lived **I**ntermediate-**L**evel **W**aste. Ag(0): metallic silver. L/ILW: **L**ow- and **I**ntermediate-**L**evel **W**aste. plasma: waste incinerated in the ZWILAG plasma plant. steel: decommissioning waste, stainless steel from reactor internals.

The waste form codes are taken from Nagra (2014a, Tab. A3.1-7).

		[mol]	[Bq]	[Sv]
All waste types		42.085	1.33×10^{15}	3.06×10^{6}
HLW total	1.24 %	0.52	1.65×10^{13}	3.79×10^{4}
HLW SF BE-L-UO2-U-HAA BE-G-UO2-U-HAA BE-B-UO2-U-HAA BE-M-UO2-U-HAA BE-G-MOX-U-HAA BE-B-MOX-U-HAA	1.11 %	0.465	1.47×10^{13}	3.39×10^{4}
HWL vitrified WA-U-KG-K1-HAA WA-F-KG-K1-HAA	0.13 %	0.055	1.75×10^{12}	4.02×10^{3}
ILW total	0.24 %	0.101	3.19×10^{12}	7.34×10^{3}
ILW Ag(0) SA-LU-MX-L3-ATA	0.23 %	0.096	3.04×10^{12}	6.99×10^{3}
ILW others	0.01 %	0.005	1.51×10^{11}	3.47×10^{2}
L/ILW total	98.52 %	41.464	1.31×10^{15}	3.02×10^{6}
L/ILW Ag(0) RA-B-MX-M2-SMA RA-G-MX-M2-SMA	**98.23 %**	**41.339**	1.31×10^{15}	3.01×10^{6}
L/ILW plasma BA-Z-PA-C1-SMA	0.17 %	0.072	2.29×10^{12}	5.28×10^{3}
L/ILW steel SA-G-ME-M2-SMA SA-B-ME-M2-SMA SA-M-ME-M2-SMA SA-L-ME-M2-SMA	0.08 %	0.034	1.07×10^{12}	2.46×10^{3}
L/ILW others	0.04 %	0.019	5.90×10^{11}	1.36×10^{3}
Total	99.95 %			

4.2 Aqueous species in pore waters

Under oxidising conditions the speciation of silver in water is fairly well known.

In pure water silver is present as Ag^+, and due to its very weak hydrolysis the species AgOH(aq) predominates only above pH 11.7, and the species $Ag(OH)_2^-$ above pH 12.6 (Brown & Ekberg 2016).

Ag^+ forms strong complexes with Cl^-, I^-, HS^- and HSe^-. The thermodynamic stability constants of AgCl(aq) and $AgCl_2^-$ are well known (Hummel 2004). The stoichiometry and stability constants of aqueous Ag – sulphide complexes are debated by the experts and no consensus has been reached yet (Stefánsson & Sewart 2003). Proposed aqueous Ag – selenide complexes originate from one experimental source and were not accepted by the NEA selenium review (Olin et al. 2005).

In the absence of sulphide and considering the generally low concentration of iodide and selenide in subsurface waters, the silver speciation in pore water under oxidising conditions is dominated by AgCl(aq) and $AgCl_2^-$ at pH < 12.

However, if the speciation and solubility of silver is calculated under reducing conditions with the data discussed above, unusual results are obtained. With decreasing redox potential metallic silver, Ag(s), becomes the thermodynamically stable solid phase and the solubility of silver in water drops to improbably low values (Fig. 12, dashed line).

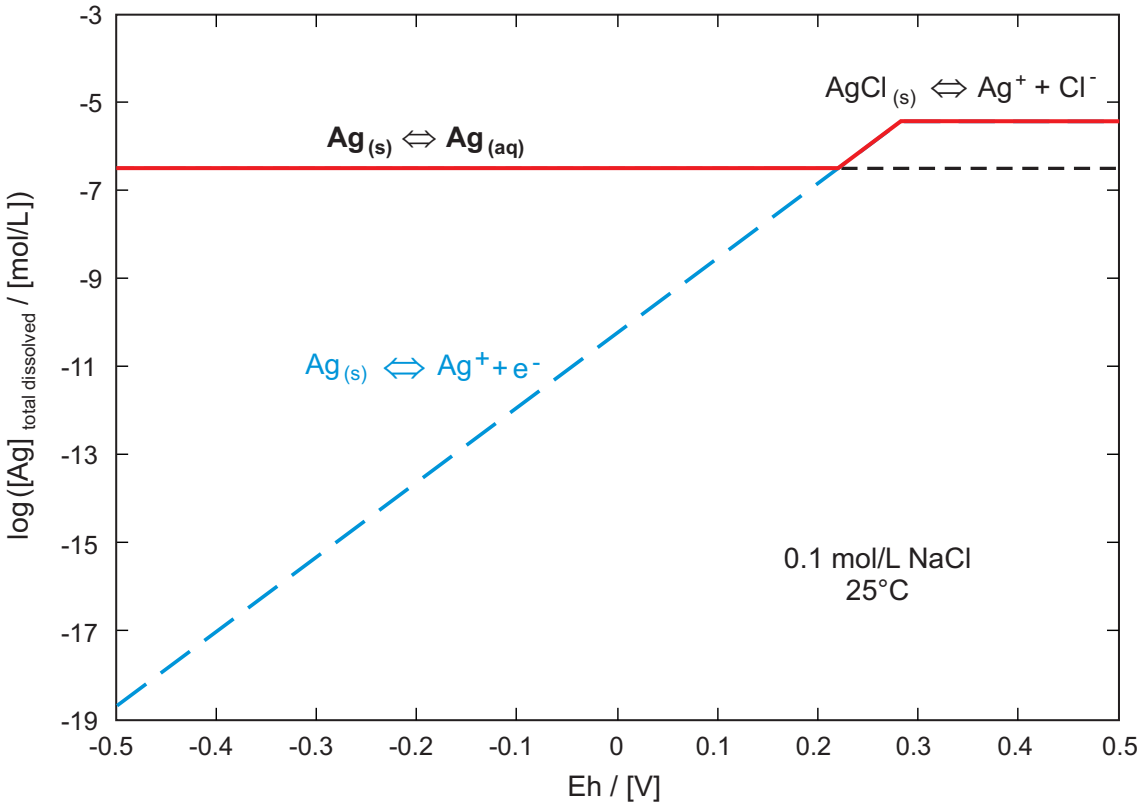

Fig. 12: Solubility of silver in water as a function of the redox potential. Solid line: total dissolved silver; dashed and dotted lines: minor dissolved silver species.

Data for Ag(cr) ⇌ Ag(aq) taken from Dobrowolski & Oglaza (1963).

This effect is similar to the "solubility abyss" discussed for the selenium system (Fig. 9) and again, the reason for this strange result is the ignorance of the dissolved element in redox state zero in all thermodynamic data bases, this time of dissolved silver in redox state zero, Ag(aq).

The chemically similar heavy metal mercury also forms strong complexes with Cl^- under oxidising conditions, and metallic mercury, Hg(l), becomes the stable phase under reducing conditions. Here, we find that the existence of the species Hg(aq) and the solubility of mercury, Hg(l) ⇌ Hg(aq), is well established (Clever et al. 1985).

By contrast, the experimental determination of the solubility of metallic silver, Ag(cr) ⇌ Ag(aq), by Kozlov & Khodakovskiy (1983) and Dobrowolski & Oglaza (1963) went unnoticed.

The mentioned strange result (Fig. 12) disappears by introducing into the database the solubility value 3.16×10^{-7} mol/L as determined by Dobrowolski & Oglaza (1963) for metallic silver according to the equilibrium

$$Ag(cr) \rightleftharpoons Ag(aq)$$

In a solution of pH 7 containing 0.1 mol/L NaCl the solubility of silver is 3.5×10^{-6} mol/L under oxidising conditions. There the solid phase is AgCl(cr) and the aqueous species are AgCl(aq) and $AgCl_2^-$. Under reducing conditions Ag(cr) becomes the thermodynamically stable phase and the solubility of silver drops to 3.2×10^{-7} mol/L. Now the dominating aqueous species is Ag(aq) (Fig.12).

However, the results obtained by Kozlov & Khodakovskiy (1983) (log K = -4.47 ± 0.03 at 200 °C and log K = -3.55 ± 0.15 at 280 °C, leading to a solubility value of 6.5×10^{-9} mol/L when extrapolated to 25 °C) and by Dobrowolski & Oglaza (1963) (a solubility value of 3.16×10^{-7} mol/L measured at 20 °C) differ by a factor of 50. Recently, the release of ^{108}Ag from irradiated pressurized water reactor control rods has been measured by gamma spectroscopy (Roth et al. 2015). After 62 and 133 days leaching under reducing conditions at room temperature the results were below detection limit. The samples were measured for around 65 hours resulting in a detection limit below ptt levels. Although the results of this study corroborate a very low silver solubility, for using the equilibrium Ag(cr) ⇌ Ag(aq) in robust safety related model calculations, an independent solubility study in the environmental temperature range is needed to remedy the mentioned discrepancy and to confirm the existence of Ag(aq) in aquatic systems.

4.3 Formation of pure solid phases

Natural occurrence of silver

Native silver, Ag(cr), and acanthite, Ag_2S(cr), are the main minerals from which silver is extracted by mining activities (Betechtin 1974). Both minerals are often found in paragenesis, i.e. they were formed together and indicate thermodynamic equilibrium at the time of their formation.

A minor silver mineral is chlorargyrite, AgCl(cr), which is found in the oxidation zone of silver mineral deposits. Considerable amounts are found in dry hot climate zones. Pseudomorphs of chlorargyrite after native silver are known, i.e. the mineral is AgCl(cr) but the appearance is that of native silver which reveals that this chlorargyrite was formed by the oxidation of Ag(cr) (Betechtin 1974).

Rare silver minerals are naumannite, α-Ag_2Se(cr) and iodargyrite, β-AgI(cr). The latter one is found in the same geochemical environment as chlorargyrite, AgCl(cr) (Betechtin 1974).

The conclusions from these field observations are:

1. Ag(cr) and Ag_2S(cr) are both formed under reducing conditions and their solubilities cannot differ by many orders of magnitude, as they are often found in paragenesis, and
2. AgCl(cr) and β-AgI(cr) are mainly reaction products formed under oxidizing conditions.

In summary, sparingly soluble pure solid phases of silver, also found in nature as minerals, are: Ag(cr), AgCl(cr), AgI(cr), Ag_2S(cr) and Ag_2Se(cr).

Ag(cr) and AgCl(cr)

In the absence of sulphide and considering the generally low concentration of iodide and selenide in subsurface waters, the most important of these solids are Ag(cr) and AgCl(cr). Their thermodynamic and kinetic behaviour has been studied in great detail in connection with the Ag-AgCl electrode.

The Ag-AgCl reference electrode, commonly used in electrochemical measurements, functions as a redox electrode and the reaction is between the silver metal, Ag(cr), and silver chloride, AgCl(cr).

The corresponding equations can be presented as follows:

$$Ag^+ + e^- \rightleftharpoons Ag(cr)$$

$$AgCl(cr) \rightleftharpoons Ag^+ + Cl^-$$

or an overall reaction can be written:

$$AgCl(cr) + e^- \rightleftharpoons Ag(cr) + Cl^-$$

The redox potential Ag(cr)/AgCl(cr) is a very accurately known electrode potential, and the stability constant of the above equilibrium is one of the most precisely known value in chemical thermodynamics (Hummel 2004).

Furthermore, this reaction is characterized by fast electrode kinetics, meaning that a sufficiently high current can be passed through the electrode with 100 % efficiency of the redox reaction (dissolution of the metal or cathodic deposition of the silver ions). The reaction has been proven to work in solutions of pH values between 0 and 13.5.

In summary, whenever equilibrium calculations suggest that Ag(cr) is the thermodynamically stable solid phase and AgCl(cr) is metastable, we can safely assume that Ag(cr) will not dissolve (if present) or will precipitate (if not present). There is no kinetic hindrance and the thermodynamic equilibria are well known.

However, the crucial data for reliable thermodynamic solubility calculations involving Ag(cr) is a reliable value for the equilibrium $Ag(cr) \rightleftharpoons Ag(aq)$, as discussed above.

4.4 Surface interactions and solid solutions

No sorption data are available for Ag^+ on cement and clay (Baeyens et al. 2014; Wieland 2014).

Although Ag^+ could be involved in ion exchange processes, strong competition of Na^+ and K^+ in cementitious systems, which is expected in stage I of the cement degradation, and the strong tendency of Ag^+ to form chloro complexes at increasing Cl^- concentration, which are expected for stages II and III of the cement degradation, suggest a distribution ratio zero (Wieland 2014).

Nothing is known about the surface interaction of dissolved silver in redox state zero, Ag(aq), with clay and cement.

Solid solutions of Ag – Cu – sulphides and more complicated systems are known as naturally occurring minerals, but no thermodynamic data are available for any of them.

4.5 Potential changes in retardation

While the neutron activation product ^{36}Cl occurs in many different waste forms, "a little bit everywhere", 98.2 % of the neutron activation product ^{108m}Ag is concentrated in one single waste form. This single waste form comprises control rods of pressurized light-water reactors consisting of an Ag-In-Cd alloy with about 80 % metallic Ag.

As more than 98 % of ^{108m}Ag is contained in metallic Ag, from the known total amounts of silver in this waste form (MIRAM 14 (Nagra 2014b): 15.8 kg per waste container", 83 waste container in total, so 1311.4 kg or 12157.45 mol in total) and the amount of activated silver (41.339 mol, Tab. 5) a mole fraction $^{108m}Ag/Ag(total)$ of 0.0034 can be determined. This could be called the "intrinsic" isotopic dilution of ^{108m}Ag because it does not depend on any external sources of stable Ag. That means, for the following considerations we can safely ignore the effect of any (unknown) traces of dissolved stable Ag in pore waters.

When the metal container and the chunks of metallic Ag corrode, a strongly reducing environment will develop. Assuming silver dissolves in redox state zero, $Ag(s) \rightleftharpoons Ag(aq)$, with a pH independent solubility of about 3×10^{-7} mol/L Ag(aq) (Dobrowolski & Oglaza 1963). Considering the "intrinsic" isotopic dilution factor 0.0034, a concentration of 1×10^{-9} mol/L $^{108m}Ag(aq)$ in the pore water of the corroding waste is expected, corresponding to 3.2×10^4 Bq/L or 0.07 mSv/L. Using the value 6.5×10^{-9} mol/L extrapolated to 25 °C from data measured at 200 and 280 °C (Kozlov & Khodakovskiy 1983) an even lower concentration of 2×10^{-11} mol/L $^{108m}Ag(aq)$ is calculated, corresponding to about 700 Bq/L or 0.002 mSv/L as the "source term" from this corroding waste form.

4.6 Conclusions and further research topics

In order to use the equilibrium $Ag(cr) \rightleftharpoons Ag(aq)$ in robust safety related model calculations, an independent solubility study in the environmental temperature range is needed to remedy the discrepancy between the two experimental solubility studies published so far, and to confirm the existence of Ag(aq) in aquatic systems.

However, if Ag(aq) is oxidized somewhere on its migration pathway it will form AgCl(aq) or $AgCl_2^-$ complexes, depending on the concentration of the ubiquitous Cl^- in pore waters. None of these species is expected to sorb significantly on mineral surfaces.

5 I-129

5.1 Origin and initial waste forms

Iodine has one stable isotope, ^{127}I, one long-lived radioactive isotope, ^{129}I, with a half-life of $(1.57 \pm 0.04) \cdot 10^7$ years, and four medium- to short-lived radioactive isotopes (^{124}I: 4.15 days, ^{125}I: 59.407 days, ^{126}I: 13.11 days, ^{131}I: 8.0252 ± 0.006 days). All other radioactive iodine isotopes have half-lives less than one day.

All of the above mentioned iodine isotopes are produced in the course of ^{235}U and ^{239}Pu fission by thermal neutrons in nuclear reactors. However, only three of them have cumulative fission yields above 10^{-6} %, i.e. ^{127}I 0.12 %, ^{129}I 0.706 %, ^{131}I 2.88 % for ^{235}U fission, and ^{127}I 0.461 %, ^{129}I 1.41 %, ^{131}I 3.72 % for ^{239}Pu fission.

The production of stable ^{127}I as fission product is of course no problem for radioactive waste disposal.

The short-lived ^{131}I can cause problems in case of an accident and it is the reason for distributing KI to the Swiss population in a certain perimeter around nuclear power plants. It is long gone when radioactive waste will be disposed of in a geological repository.

The radioactive isotope relevant for long-term safety is ^{129}I; and unfortunately it is the one with by far the longest half-life of all important fission products (Fig. 2) and the fission product with the least favourable chemistry with respect to retardation in the multiple safety barrier system of a geological repository.

As a little bonus, ^{129}I decays by simple beta minus decay (β-) to stable ^{129}Xe, a noble gas with no health hazards.

In Swiss radioactive waste, 99.5 % of the ^{129}I activity is found in spent nuclear fuel (Fig. 13). In contrast to ^{79}Se, the other fission product discussed here, very low amounts of iodine are found in vitrified HLW (0.38 %, Fig. 13). The volatile iodine largely got lost to the atmosphere and to the sea during the reprocessing steps of the dissolved spent nuclear fuel; only about 0.1 % of the original amount is left in HLW glass. Originally, all Swiss spent nuclear fuel was sent to reprocessing facilities, and vitrified high-level waste had to be taken back, but a 10-year moratorium on reprocessing lead to increasing amounts of spent fuel for direct disposal. The total amount of ^{129}I to be disposed of is strongly affected by the moratorium, in absolute quantities about 20 mol ^{129}I from reprocessing (HLW vitrified, Tab. 6) versus about 5'000 mol from direct disposal (HLW SF, Tab. 6).

^{129}I in low-level wastes (L/ILW) is mainly found in ion exchange resins (93 %) (Fig. 13). These ion-exchange resins have been used for decontamination procedures during reactor operation.

Nothing is known about the chemical form of ^{129}I any of these waste forms.

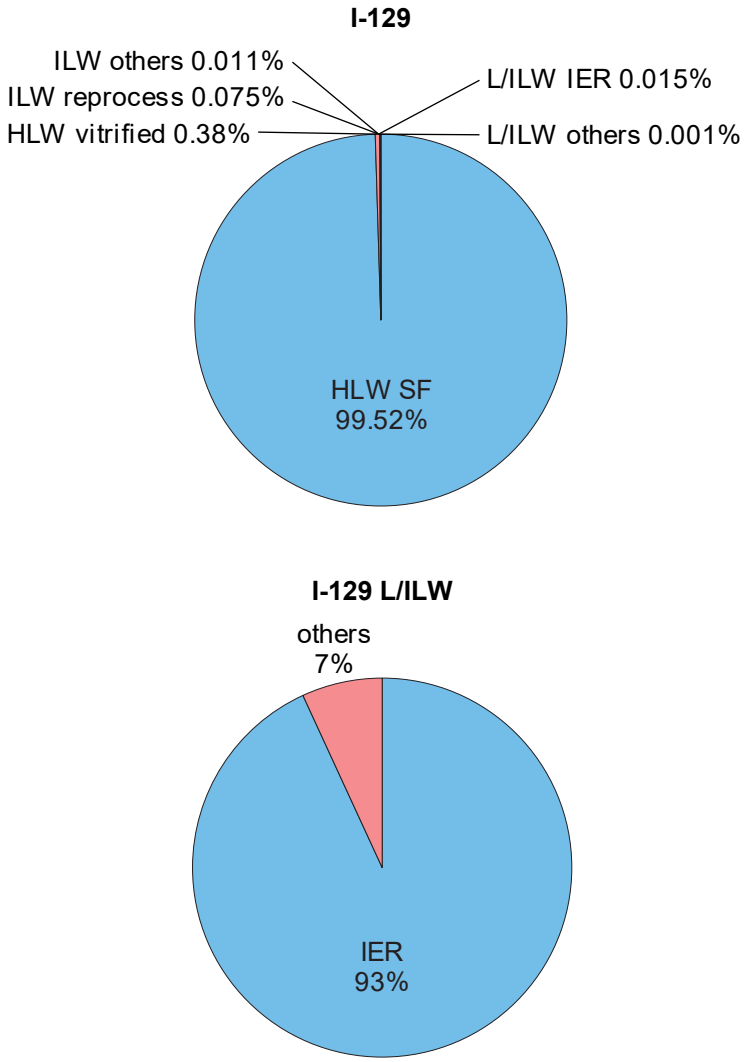

Fig. 13: Distribution of ^{129}I to different waste forms in mole percent according to MIRAM 14 (Nagra 2014b). Top: Total of all waste forms. Bottom: Low- and intermediate-level waste only.

The abbreviations are HLW: **H**igh-**L**evel **W**aste. SF: **S**pent nuclear **F**uel assemblies. vitrified: vitrified HLW from reprocessing of spent fuel. ILW: long-lived **I**ntermediate-**L**evel **W**aste. reprocess: ILW from reprocessing (compacted hulls and ends, vitrified sludges). L/ILW: **L**ow- and **I**ntermediate-**L**evel **W**aste. IER: **I**on-**E**xchange **R**esins.

Tab. 6: Distribution of ^{129}I to different waste forms according to MIRAM 14 (Nagra 2014b). Original data in [Bq], converted to [mol] assuming $T½ = 1.57 \times 10^7$ years, converted to [Sv] using 1.1×10^{-7} [Sv/Bq].

The abbreviations are HLW: **H**igh-**L**evel **W**aste. SF: **S**pent nuclear **F**uel assemblies. vitrified: vitrified HLW from reprocessing of spent fuel. ILW: long-lived **I**ntermediate-**L**evel **W**aste. reprocess: ILW from reprocessing (compacted hulls and ends, vitrified sludges). L/ILW: **L**ow- and **I**ntermediate-**L**evel **W**aste. IER: **I**on-**E**xchange **R**esins.
The waste form codes are taken from Nagra (2014a, Tab. A3.1-7).

		[mol]	[Bq]	[Sv]
All waste types		5'096.68	4.29×10^{12}	4.72×10^5
HLW total	99.90 %	5'091.49	4.29×10^{12}	4.72×10^5
HLW SF BE-L-UO2-U-HAA BE-G-UO2-U-HAA BE-B-UO2-U-HAA BE-M-UO2-U-HAA BE-G-MOX-U-HAA BE-B-MOX-U-HAA	**99.52 %**	**5'072.36**	4.27×10^{12}	4.70×10^5
HLW vitrified WA-F-KG-K1-HAA WA-U-KG-K1-HAA	0.38 %	19.13	1.61×10^{10}	1.77×10^3
ILW total	0.086 %	4.37	3.68×10^9	405
ILW reprocess WA-F-MX-K1-ATA WA-F-SG-K1-ATA	0.075 %	3.82	3.22×10^9	354
ILW others	0.011 %	0.55	4.59×10^8	51
L/ILW total	0.016 %	0.82	6.90×10^8	76
L/ILW IER SA-M-H-M2-SMA BA-M-H-F2-SMA SA-L-H-M2-SMA BA-L-H-F2-SMA BA-B-HP-F2-SMA BA-B-HP-F1-SMA BA-G-HB-F2-SMA SA-B-H-M2-SMA SA-G-H-M2-SMA	0.015 %	0.76	6.43×10^8	71
L/ILW others	0.001 %	0.06	4.73×10^7	5
Total	99.99 %			

5.2 Aqueous species and pure solid phases

Iodine occurs in aqueous solutions of environmental concern mainly as iodide, I^-. Other thermodynamically stable forms of iodine in water are $I_2(aq)$, I_3^- and IO_3^-.

Elemental iodine is a solid, $I_2(cr)$, with a melting point of 113.7 °C. $I_2(cr)$ is slightly soluble in water as $I_2(aq)$, with about 0.3 g/kg_{H2O} at 20 °C and 0.8 g/kg_{H2O} at 50 °C.

The only important polyiodide anion in aqueous solution is the linear triiodide, I_3^-. Its formation explains why the solubility of elemental iodine in water may be increased by the addition of e.g. potassium iodide solution:

$$I_2(aq) + I^- \rightleftharpoons I_3^-$$

Hypoiodous acid, HIO(aq) is unstable to disproportionation. Hypoiodite ions, IO^-, when formed disproportionate immediately to give iodide and iodate:

$$3\ IO^- \rightleftharpoons 2\ I^- + IO_3^-$$

Iodous acid, $HIO_2(aq)$ and iodite, IO_2^-, are even less stable and only exist as a fleeting intermediate in the oxidation of iodide to iodate, if at all.

Periodates are known, including the tetrahedral IO_4^-; they are powerful oxidising agents, e.g. quickly oxidising Mn^{2+} to MnO_4^-.

An Eh – pH predominance diagram for iodine species in water at 25 °C (Fig. 14) shows a large stability field of iodide, I^-, and iodate, IO_3^-, is only stable under oxidising conditions. In neutral to acidic solutions also dissolved iodine, $I_2(aq)$, is found under oxidising conditions.

The interaction of iodide, I^-, with cations is similar to the already discussed interactions for chloride. Specifically, the interaction of I^- with all "hard" cations, including lanthanides and actinides, is described in thermodynamic models as weak complexation and/or specific ion interaction, whereas I^- forms strong complexes with "soft" metal cations like Ag, Cu, Hg and Pb.

Iodide forms highly soluble salts with all major and minor components of ground and surface waters; all alkali and alkaline earth elements, iron, manganese, nickel, aluminium.

By contrast, iodide forms sparingly to slightly soluble solid phases with "soft" metal cations, e.g. Hg_2I_2, AgI, CuI, PbI_2. The solid phases are listed in the order of increasing solubility products, e.g.

$$AgI(cr) \rightleftharpoons Ag^+ + I^- \qquad K_{s,0} = 9.1 \times 10^{-17}$$

$$CuI(cr) \rightleftharpoons Cu^+ + I^- \qquad K_{s,0} = 1.1 \times 10^{-12}$$

$$PbI_2(cr) \rightleftharpoons Pb^{2+} + 2I^- \qquad K_{s,0} = 2.1 \times 10^{-9}$$

However, considering solubility products only is misleading because iodide also forms strong aqueous complexes with the same "soft" metal cations and hence, the total solubility of these compounds is generally much higher than the solubility products alone would suggest.

For PbI_2(cr) the solubility in water at 20 °C is 0.7 g/kg_{H2O}, and for CuI(cr) 0.04 g/kg_{H2O}. These solids are slightly soluble. The only sparingly soluble solid is AgI(cr) with a solubility in water of 3×10^{-6} g/kg_{H2O} at 20 °C.

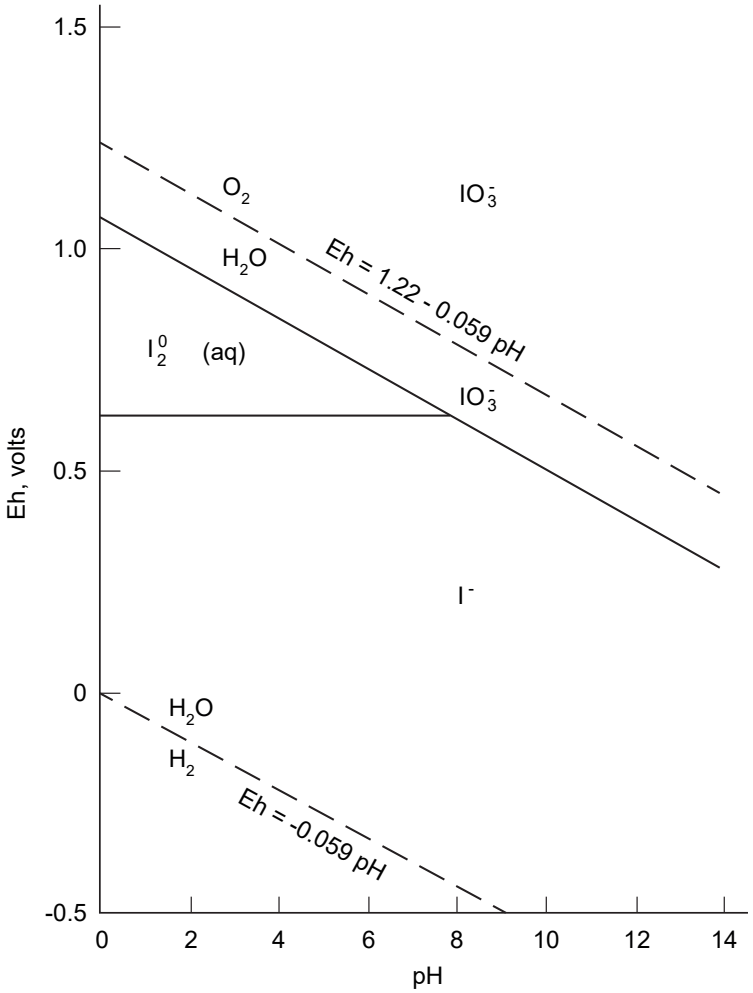

Fig. 14: Eh – ph predominance diagram for iodine species in water at 25 °C. The domain of H_2O stability is indicated by the dashed lines.

Taken from Liu & von Gunten (1988).

5.3 Surface interactions and solid solutions

Cement

Iodide, I^-, and iodate, IO_3^-, are the reduced and oxidized forms of inorganic iodine within the stability field of water in cementitious systems (Fig. 14). While IO_3^- should be the dominant chemical form of iodine in oxidised chemical systems, spectroscopic investigations of I^- uptake by HCP (prepared from HTS cement) did not indicate oxidation of I^- to IO_3^- (Wieland 2014).

Numerous studies on the interaction of HCP and cement minerals have been reported over the last 30 years, but the chemical processes controlling I^- interaction with HCP are still poorly understood. The generally very weak sorption effects can be ranked in decreasing order from AFm > C-S-H with high C/S ratio ≈ AFt > C-S-H with low C/S ratio. Recent LES in-house studies with ^{125}I on selected cement minerals largely support this sequence. AFm-SO_4, $3CaO{\cdot}Al_2O_3{\cdot}CaSO_4{\cdot}11H_2O$, was found to exhibit the largest sorption potential while I^- binding to C-S-H with high C/S ratios (C/S > 1) was much weaker (Wieland 2014).

Recent LES in-house studies on I^- uptake by AFm phases confirmed the formation of AFm-I_2 ($3CaO{\cdot}Al_2O_3{\cdot}CaI_2{\cdot}12H_2O$) at high iodide concentrations (Aimoz et al. 2012a), thus supporting observations made in earlier studies. In addition, however, it was observed that I^- strongly binds onto AFm-SO_4 as the latter phase is capable of taking up the anion into the interlayer in contrast to ettringite and other AFm-type minerals, such as monocarbonate (AFm-CO_3) and Friedel's salt (AFm-Cl_2). In thermodynamic terms I^- uptake by AFm-SO_4 could be modelled as solid solution formation between AFm-SO_4/AFm-I_2 end members (Aimoz et al. 2012b). The study by Aimoz et al. (2102a) further shows that CO_3^{2-} and Cl^- are competing anions which significantly reduce I^- uptake be AFm phases. High concentrations of the competing anions in cementitious systems promote conversion of AFM-SO_4 to AFm-CO_3 or AFm-Cl_2, which may strongly reduce I^- sorption capacity of HCP. Therefore, the presence or absence of AFM-SO_4 in the cement paste has a major impact on its capacity to retard I^- (Wieland 2014).

Clay systems

Glaus et al. (2008) studied the through- and out-diffusion behaviour of $^{125}I^-$ and $^{125}IO_3^-$ in an intact sample of Opalinus Clay (OPA) from the Benken drilling site (Switzerland). An effective diffusion coefficient, $D_e = (4.5 \pm 0.5){\cdot}10^{-12}$ m^2 s^{-1}, and a rock capacity factor, $\alpha = 0.04 \pm 0.01$, were measured in the through-diffusion experiments with $^{125}I^-$. The latter result shows that no sorption of I^- takes place in OPA because in previous work the same rock capacity factor was measured for the non-sorbing Cl^- tracer.

No break-through of $^{125}IO_3^-$ could be observed by Glaus et al. (2008) in the through diffusion experiment with $^{125}IO_3^-$ as the source species. Instead a flux of $^{125}I^-$ into the target reservoir was substantiated. This observation showed that IO_3^- was rapidly converted to I^- upon contact with OPA. The transformation was presumably mediated by unidentified reducing components of OPA.

The uptake of iodide, I^-, on natural pyrite was investigated by Aimoz et al. (2011) under nearly anoxic conditions (O_2 < 5 ppm) over a wide concentration range (10^{-11} – 10^{-3} mol/L total I^-) using $^{125}I^-$ as the radioactive tracer. Weak but measurable sorption was observed; distribution coefficients (R_d) were less than 0.002 m^3 kg^{-1} and decreased with increasing total iodide concentration. Iodide sorption was connected to the presence of oxidised clusters on the pyrite surface, which were presumably formed by the reaction with limited amounts of dissolved

oxygen. The results obtained indicated that pyrite cannot be considered as an effective scavenger of ^{129}I under the geochemical conditions prevailing in geological repositories.

5.4 Potential changes in retardation

The formation of the sparingly soluble solid AgI(cr) is a potential "sink" for dissolved iodide. However, several reasons render iodide solubility limitation by AgI(cr) formation improbable:

1. 99.5 % of the ^{129}I activity is found in SF (Fig. 13) while 98.2 % of the ^{108m}Ag activity is found in L/ILW waste (Fig. 11). Hence, the large masses of iodine (about 5'000 mol, Tab. 6) and silver (about 12'000 mol, see chapter 4.5) will go to different geological repositories and thus, they never will "meet" to form AgI(cr).
2. If we consider SF alone and assume the same "intrinsic" isotopic dilution factor $^{108m}Ag/Ag(total) = 0.0034$ as derived for L/ILW (chapter 4.5) we have about 5'000 mol iodide versus about 140 mol Ag(total) (from 0.465 mol ^{108m}Ag in SF, Tab. 5). Hence, by pure mass balance considerations AgI(cr) cannot act as a sink for iodide in SF.
3. If we consider L/ILW alone the mass balance would be in favour of solubility limitation by AgI(cr) precipitation: about 12'000 mol Ag(total) versus about 0.8 mol ^{129}I (Tab. 6). However, 93 % of this ^{129}I is found in a completely different waste form than ^{108m}Ag (ion-exchange resins versus reactor steel, Figs. 13 and 11) and they will go to different compartments in an L/ILW geological repository. Assuming a "global mixing tank" is not a robust model here for safety assessment calculations. But even if we do a "global mixing tank" model, Ag(cr) will be the thermodynamically stable phase under reducing conditions and AgI(cr) will not form, or if formed will transform to Ag(cr) and release the bound I^- again. In the presence of sulphide in the pore water of the near-field, AgI(cr), even if it had formed, may be substituted by Ag_2S(cr) and this process also will release the bound I^-.

In cementitious systems AFm-I_2 ($3CaO \cdot Al_2O_3 \cdot CaI_2 \cdot 12H_2O$) can form at high iodide concentrations in solution, and solid solution formation between AFm-SO_4/AFm-I_2 end members has been observed at lower iodide concentrations. However, CO_3^{2-} and Cl^- are competing anions which significantly reduce I^- uptake be AFm phases and high concentrations of the competing anions in cementitious systems promote the conversion of AFM-SO_4 to AFm-CO_3 or AFm-Cl_2, which may strongly reduce the I^- sorption capacity of hardened cement paste. AFm-I_2 and AFm-SO_4/AFm-I_2 solid solutions are scientifically very interesting systems to study but they will hardly change the retardation of iodide in the cementitious near-field.

The uptake of iodide on natural pyrite was found to be weak which indicated that pyrite cannot be considered as an effective scavenger of ^{129}I under the geochemical conditions prevailing in geological repositories.

No sorption of I^- in Opalinus Clay could be observed.

5.5 Conclusions and further research topics

At the end of this journey in iodide (geo)chemistry it seems improbable that hitherto major chemical solubility and retardation phenomena have been overlooked. No promising future research topics for iodine retardation could be identified.

6 Remaining uncertainties

Cl-36

Considering the chemical behaviour of the chloride anion in pore waters, the large isotopic dilution of ^{36}Cl by stable ^{35}Cl and ^{37}Cl in the near- and far-field of a deep geological repository, and the long half-life of ^{36}Cl, no significant retardation effects are expected for ^{36}Cl. It seems also improbable that hitherto major chemical solubility and retardation phenomena have been overlooked.

However, it might be worthwhile to have a closer look at the source term to further bound the inventory and resulting dose rate from Cl-36.

^{36}Cl is the only safety relevant radionuclide discussed here whose inventory is solely based on measured or mere assumed trace concentrations of its stable isotopes which are impurities in nuclear fuel and structural reactor material.

The calculated concentrations of activated ^{36}Cl might be overestimated by orders of magnitude because they depend on very few measurements and many (pessimistic) assumptions about ^{35}Cl trace concentrations in nuclear fuel, reactor steel and other metallic compounds.

Hence, a re-assessment of the ^{36}Cl inventory in spent fuel, cladding and stainless steel can further increase reliability of the dose curves and reduce uncertainties.

Se-79

The chemical form of selenium released from the most important waste forms is expected to be very similar:

SF	(Se in UO_2 matrix + corroding steel canister)	$Fe(0) \rightarrow Fe^{2+}$, $Se(-II) \rightarrow HSe^-$ (Se(aq))
HLW	(Se in glass matrix + corroding steel canister)	$Fe(0) \rightarrow Fe^{2+}$, $Se(IV) \rightarrow$ Se(aq), HSe^-
L/ILW	(Se in corroding reactor steel)	$Fe(0) \rightarrow Fe^{2+}$, $Se(?) \rightarrow$ Se(aq), HSe^-

However, the speciation of the selenium – water system is incomplete, especially in near-neutral conditions. The species Se(aq), dissolved selenium in redox state zero, has not been considered in any study so far, and the lowest attainable solubility of Se(cr) in near-neutral solutions is unknown. Besides Se(aq), selenium polymers longer than the tetramer might exist in these solutions, and their polymerisation equilibria and the protonation constants of these polymers need to be determined.

A potential sink for dissolved Se in the near-field is the formation of ferroselite, $FeSe_2$(cr). However, no information at all is available concerning aqueous Fe(II) – selenide complexes and thus, the solubility of $FeSe_2$(cr) in water cannot be calculated from existing thermodynamic data.

Recently it has been shown that pyrite, FeS_2(cr), and its most important precursor phase mackinawite, FeS(cr), are efficient in removing selenium from solution by forming $FeSe_xS_y$ solid solutions. Probably Se(0) is incorporated or formed as a separate phase. The formation of these solid solutions may lead to much lower selenium solubilities as the formation of the pure ferroselite, $FeSe_2$(cr). However, no reliable solubility studies have been published so far and the effect of selenium removal from solution by $FeSe_xS_y$ formation cannot be quantified yet.

In summary, the uncertainties regarding the aqueous selenium chemistry in reducing environments and the resulting selenium solubility could be reduced by:

- Experimental and modelling studies of the system Se(cr) ⇌ Se(aq), including the formation of polyselenides (HSe_x^-) and
- Experimental and modelling studies of the formation and solubility of $FeSe_2$(cr) and $FeSe_xS_y$ solid solutions

Ag-108m

While the neutron activation product ^{36}Cl occurs in many different waste forms, "a little bit everywhere", 98.2 % of the neutron activation product ^{108m}Ag is concentrated in one single waste form. This single waste form comprises control rods of pressurized light-water reactors consisting of an Ag-In-Cd alloy with about 80 % metallic Ag. From the known total amounts of silver in this waste form (about 12'000 mol in total) and the amount of activated silver (about 41 mol) a mole fraction $^{108m}Ag/Ag(total)$ of 0.0034 can be determined. This is the "intrinsic" isotopic dilution of ^{108m}Ag.

If the metal container and the chunks of metallic Ag corrode, a strongly reducing environment will develop. Silver dissolves then in redox state zero, Ag(cr) ⇌ Ag(aq), with a pH independent solubility of about 3×10^{-7} mol/L Ag(aq) (Dobrowolski & Oglaza 1963). Considering the intrinsic isotopic dilution factor 0.0034, a concentration of 1×10^{-9} mol/L $^{108m}Ag(aq)$ in the pore water of the corroding waste is expected. Using the value 6.5×10^{-9} mol/L extrapolated to 25 °C from data measured at 200 and 280 °C (Kozlov & Khodakovskiy 1983) an even lower concentration of 2×10^{-11} mol/L $^{108m}Ag(aq)$ is calculated as the "source term" from this corroding waste form.

The results obtained by Kozlov & Khodakovskiy (1983) and by Dobrowolski & Oglaza (1963) differ by a factor of 50. In order to use the equilibrium

$$Ag(cr) \rightleftharpoons Ag(aq)$$

in robust safety related model calculations, an independent solubility study in the environmental temperature range would be needed to remedy the mentioned discrepancy and to confirm the existence of Ag(aq) in aquatic systems.

Such a study concerning silver dissolving in redox state zero, Ag(cr) ⇌ Ag(aq), would also have consequences for modelling the dissolution behaviour of Cu, Ni and Pd under reducing conditions.

I-129

It seems improbable that hitherto major chemical solubility and retardation phenomena have been overlooked. It is thus also unlikely that uncertainties regarding iodine retardation can be reduced.

7 References

Aimoz, L., E., Curti, E. & Mäder, U. (2011): Iodide interaction with natural pyrite. J. Radioanal. Nucl. Chem. 288, 517-524.

Aimoz, L., Kulik, D.A., Wieland, E., Curti, E., Lothenbach, B. & Mäder, U. (2012b): Thermodynamics of AFm-(I_2,SO_4) solid solution and of its end-members in aqueous media. Applied Geochemistry 27, 2117-2129.

Aimoz, L., Wieland, E., Taviot-Guého, C., Dähn, R., Vespa, M. & Churakov, S. (2012a): Structural insights into iodide uptake by AFm phases. Environmental Science and Technology 46, 3874-3881.

Aitchison, I. & Davies, P.H. (1993): Role of microsegregation in fracture of cold-worked Zr–2.5Nb pressure tubes. Journal of Nuclear Materials 203, 206-220.

Baeyens, B., Thoenen, T., Bradbury, M.H. & Marques Fernandes, M. (2014): Sorption data bases for argillaceous rocks and bentonite for the provisional safety analyses for SGT-E2. Nagra Technical Report NTB 12-04.

Berner, U. (2014a): Solubility of radionuclides in a bentonite environment for provisional safety analyses for SGT-E2. Nagra Technical Report NTB 14-06.

Berner, U. (2014b): Solubility of radionuclides in a concrete environment for provisional safety analyses for SGT-E2. Nagra Technical Report NTB 14-07.

Betechtin, A.G. (1974): Lehrbuch der speziellen Mineralogie. VEB Deutscher Verlag für Grundstoffindustrie, Leipzig, 6. Aufl., 683pp.

Boulegue, J. (1978): Solubility of Elemental Sulfur in Water at 298 K. Phosphorus and Sulfur 5, 127-128.

Brown, P.L. & Ekberg, C. (2016): Hydrolysis of Metal Ions. Wiley-VCH Verlag GmbH & Co. KGaA, Weinhime, Germany, 917 pp.

Calmet, D.; Coreau, N.; Germain, P.; Goutelard, F.; Letessier, P.; Frechou, C.; Maro, D. (2001): Chlorine-36 measurement in the near-field environment of a spent nuclear fuel reprocessing plant. Radiochemical Measurements Conference (BAER Conference), Honolulu, 2001.

Clever, H.L., Johnson, S.A. & Derrick, M.E. (1985): The solubility of mercury and some sparingly soluble mercury salts in water and aqueous electrolyte solutions. J. Phys. Chem. Ref. Data 14, 631-679.

Curti, E., Aimoz, L. & Kitamura, A. (2013): Selenium uptake onto natural pyrite. J. Radioanal. Nucl. Chem. 295, 1655-1665.

Curti, E., Froideval-Zumbiehl, A., Günther-Leopold, I., Martin, M., Bullemer, A., Linder, H., Borca, C.N. & Grolimund, D. (2014): Selenium redox speciation and coordination in high-burnup UO_2 fuel: Consequences for the release of ^{79}Se in a deep underground repository. Journal of Nuclear Materials 453, 98-106.

Curti, E., Puranen, A., Grolimund, D., Jädernas, D., Sheptyakov, D. & Mesbah, A. (2015): Characterization of selenium in UO_2 spent nuclear fuel by micro X-ray absorption spectroscopy and its thermodynamic stability. Environmental Science: Processes & Impacts 17, 1760-1768.

Dardenne, K., González-Robles, E., Rothe, J., Müller, N., Christill, G., Lemmer, D., Praetorius, R., Kienzler, B., Metz. V., Roth, G. & Geckeis, H. (2015): XAS and XRF investigations of an actual HAWC glass fragment obtained from the Karlsruhe vitrification plant (VEK). Journal of Nucelar Materials 460, 209-215.

Diener, A. & Neumann, T. (2011): Synthesis and incorporation of selenide in pyrite and mackinawite. Radiochimica Acta 99, 791-798.

Diener, A., Neumann, T., Kramar, U. & Schild, B. (2012): Structure of selenium incorporated in pyrite and mackinawite as determinde by XAFS analyses. Journal of Contaminant Hydrology 133, 30-39.

Dobrowolski, J. & Oglaza, J. (1963): Zastoswanie izotopu ^{110}Ag do badania rozpuszczalnosci srebra metalicznego i chlorku srebra w roztworach wodnych siarczanu cynku [use of the isotope ^{110}Ag in studying the solubility of silver metal and silver chloride in aqueous solutions of zinc sulphide]. Nucleonika 8, 79-81 (in Polish).

Evans, J.C., Lepel, E.L., Sanders, R.W., Wilkerson, C.L., Silker, W., Thomas, C.W., Abel, K.H. & Robertson, D.R. (1984): Long-lived activation products in reactor materials. Pacific Northwest Laboratory, Report NUREG/CR-3474, 185pp.

Felipe-Sotelo, M., Hinchliff, J., Drury, D., Evans, N.D.M., Williams, S. & Read D. (2014): Radial diffusion of radiocaesium and radioiodide through cementitious backfill. Physics and Chemistry of the Earth 70-71, 60-70.

Finck, N. & Dardenne, K. (2016): Interaction of selenite with reduced Fe and/or S species: An XRD and XAS study. Journal of Contaminant Hydrology 188, 44-51.

Finck, N., Dardenne, K., Bosbach, D. & Geckeis, H. (2012): Selenide retention by mackinawite. Environ. Sci. Technol. 46, 10004-10011.

Glaus, M.A., Müller, W. & Van Loon, L.R. (2008): Diffusion of iodide and iodate through Opalinus Clay: Monitoring of the redox state using an anion chromatographic technique. Applied Geochemistry 23, 3612-3619.

Hou, X., Østergaard, L.F. & Nielsen, S. (2007): Determination of 36Cl in nuclear waste from reactor decommissioning. Analytical Chemistry 79, 3126-3134.

Hummel, W. (2004): The influence of cyanide complexation on the speciation and solubility of radionuclides in a geological repository. Environmental Geology 45, 633-646,

Iida, Y., Yamaguchi, T., Tanaka, T. & Nakayama, S. (2010): Solubility of Selenium at High Ionic Strength under Anoxic Conditions. Journal of Nuclear Science and Technology 47, 431-438.

Kamyshny, Jr., A. (2009): Solubility of cyclooctasulfur in pure water and sea water at different temperatures. Geochim. Cosmochim. Acta 73, 6022-6028.

Kamyshny, Jr., A., Goifman, A., Gun, J., Rizkov, D. & Lev, O. (2004): Equilibrium Distribution of Polysulfide Ions in Aqueous Solutions at 25°C: A new Approach for the Study of Polysulfides' Equilibria. Environ. Sci. Technol. 38, 6633-6644.

Kozlov, V.K. & Khodakovskiy, I.L. (1983): The thermodynamic parameters of atomic silver in aqueous solution at 25-280 °C. Geochemistry International 20, 118-131 (translated from Geokhimiya 6 (1983) 836-848).

Liu, Y. & von Gunten, H.R. (1988): Migration chemistry and behaviuor of iodine relevant to geological disposal of radioactive wastes – a literature review with a compilation of sorption data. Nagra Technical Report NTB 88-29.

Mäder, U. (2009): Reference pore water for the Opalinus Clay and "Brown Dogger" for the provisional safety-analysis in the framework of the sectoral plan – interim results (SGT-ZE). Nagra Arbeitsbericht NAB 09-14.

Nagra (2014a): Provisorische Sicherheitsanalysen für SGT Etappe 2: Elektronischer Daten- und Resultateordner (EDR). Nagra Arbeitsbericht NAB 14-36.

Nagra (2014b): Modellhaftes Inventar für radioaktive Materialien MIRAM 14. Nagra Technischer Bericht NTB 14-04.

Ochs, M., Lothenbach, B. & Giffault, E. (2002): Uptake of oxo-anions by cements through solid-solution formation: experimental evidence and modelling. Radiochimica Acta 90, 639-646.

Olin, Å., Noläng, B., Öhman, L.-O., Osadchii, E.G. & Rosén E. (2005): Chemical Thermodynamics Vol. 7: Chemical Thermodynamics of Selenium (OECD Nuclear Energy Agency, ed.) Elsevier, Amsterdam, The Netherlands, 851 pp.

Pipon, Y., Toulhoat, N., Moncoffre, N., Raimbault, L., Scheidegger, A.M., Farges, F. & Carlot, G. (2007): Thermal diffusion of chlorine in uranium dioxide studied by secondary ion mass spectrometry and X-ray absorption spectroscopy. Journal of Nuclear Materials 362, 416-425.

Rao, B., Hatzinger, P.B., Bohlke, J.K., Sturchio, N.C., Andraski, B.J., Eckardt, F.D. & Jackson, W.A. (2010): Natural chlorate in the environment: Application of a new IC-ESI/MS/MS method with a $Cl^{18}O_3^-$ internal standard. Environ. Sci. Technol. 44, 8429-8434.

Robertson, D.E., Thomas, C.W., Pratt, S.L., Lepel, E.A. & Thomas, V.W. (2000): Low-level radioactive waste classification, characterization, and assessment: Waste streams and neutron-activated metals. NUREG/CR-6567 PNNL-11659. U.S. Nuclear Regulatory Commission Office of Nuclear Regulatory Research, Washington.

Roth, O., Granfors, M., Puranen, A. & Spahiu, K. (2015): Release of ^{108}Ag from Irradiated PWR Control Rod Absorbers under Deep Repository Conditions. Mater. Res. Soc. Symp.Proc. Vol. 1744, 217-222.

Sheppard, S.C. & Herod, M. (2012): Variation in background concentrations and specific activities of ^{36}Cl, ^{129}I and U/Th-series radionuclides in surface waters. Journal of Environmental Radioactivity 106, 27-34.

Sheppard, S.C., Johnson, L.H., Goodwin, B.W., Tait, J.C., Wuschke, D.M. & Davison, C.C. (1996): Chlorine-36 in nuclear waste disposal – 1. Assessment results for used fuel with comparison to ^{129}I and ^{14}C. Waste Management 16, 607-614.

Stefánsson, A. & Seward, T.M. (2003): Experimental determination of the stability and stoichiometry of sulphide complexes of silver(I) in hydrothermal solutions to 400 °C. Geochimica et Cosmochimica Acta 67, 1395-1413.

Tait, J.C., Cornett, R.J.J., Chant, L.A., Jirovec, J., McConnell, J. & Wilkin, D.L. (1997): Determination of Cl impurities and ^{36}Cl instant release from used CANDU fuels, Mat.Res. Soc. Symp. Proc. 465, 503-510, Materials Research Society, Pittsburgh, PA.

Traber Daniel, Blaser Petra (2013): Gesteinsparameter der Wirtgesteine Opalinuston, 'Brauner Dogger', Effinger Schichten und Helvetische Mergel als Grundlage für die Sorptions-datenbank. Nagra Arbeitsbericht NAB 12-39.

Van Es, E., Hinchliff, J., Felipe-Sotelo, M., Milodowski, A.E., Field, L.P., Evans, N.D.M. & Read, D. (2015): Retention of Chlorine-36 by a cementitious backfill. Mineralogical Magazine 79, 1297-1305.

Van Loon, L. (2014): Effective diffusion coefficients and porosity values for argillaceous rocks and bentonite: measured and estimated values for the provisional safety analyses for SGT-E2. Nagra Technical Report NTB 12-03. Nagra, Wettingen.

Wang, F. & Tessier, A. (2009): Zero-Valent Sulfur and Metal Speciation in Sediment Porewaters of Freshwater Lakes. Environ. Sci. Technol. 43, 7252-7257.

Wieland, E. & Hummel, W. (2015): Formation and stability of ^{14}C-containing organic compounds in alkaline iron-water systems: preliminary assessment based on a literature survey and thermodynamic modelling. Mineralogical Magazine 79, 1275-1286.

Wieland, E. (2014): Sorption data base for the cementitious near field of L/ILW and ILW repositories for provisional safety analyses for SGT-E2. Nagra Technical Report NTB 14-08. Nagra, Wettingen.

Zreda, M.G., Phillips, F.M., Elmore, D., Kubik, P.W., Sharma, P. & Dorn, R.I. (1991): Cosmogenic chlorine-36 production rates in terrestrial rocks. Earth and Planetary Science Letters 105, 94.109.

Acknowledgements

The author would like to thank V. Cloet (Nagra) for providing access to MIRAM 14, for valuable input to the introduction, for reviewing several versions of the manuscript and for continuous support and encouragement to finish this report, and K. Spahiu (SKB) for carefully reviewing the final manuscript and providing valuable comments which clarified and improved many details of the report.

Appendix: Discussion of selected references

Iida, Y., Yamaguchi, T., Tanaka, T. & Nakayama, S. (2010): Solubility of Selenium at High Ionic Strength under Anoxic Conditions. Journal of Nuclear Science and Technology 47, 431-438.

Iida et al. (2010) measured the solubility of selenium, Se(cr), in the pH range 5 to 13. Above pH 9 their results are fairly consistent with the dataset of Olin et al. (2005) (Fig. A1). However, below pH 9 they measured significantly higher total dissolved selenium concentrations than predicted with the dataset of Olin et al. (2005) (Fig. A1).

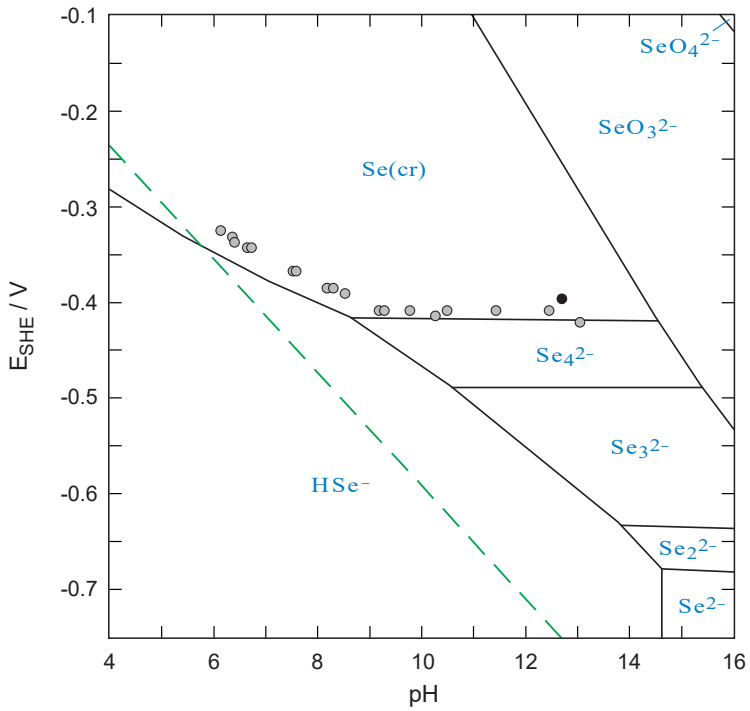

Fig. A1: Predominance diagram of selenium species in "pure" water as a function of pH and redox conditions (E_{SHE} refers to the standard hydrogen electrode, in volts), $[Se]_{total} = 2 \times 10^{-2}$ mol dm^{-3}, T = 25 °C, ionic strength I = 0.1 mol dm^{-3}. The dashed line indicates the stability limits of water.

Thermodynamic data taken from Olin et al. (2005). Experimental solubility data at $[Se]_{total} \approx 2 \times 10^{-2}$ mol dm^{-3} taken from Iida et al. (2010); grey circles: from oversaturation, black circle: from undersaturation.

In order to explain this Iida et al. (2010) postulated a phase transition from Se(cr) to an amorphous selenium phase Se(am) with a higher solubility than Se(cr) below pH 9, although they found Se(cr) by X-ray powder diffraction in all cases (red lines below pH 9 in Fig. A2). In addition they slightly adjusted the thermodynamic constant for the tetraselenide Se_4^{2-} (red lines above pH 9 in Fig. A2). The latter adjustments are no problem as the stability constants of the polyselenides have been experimentally determined in 0.5 – 2 M KOH solutions at pH > 13 and thus, the stability region of Se_4^{2-} might be underestimated. However, there is no independent evidence for the formation of an amorphous selenium phase below pH 9 and the presence of Se(cr) in all experiments of Iida et al. (2010) contradicts this model assumption.

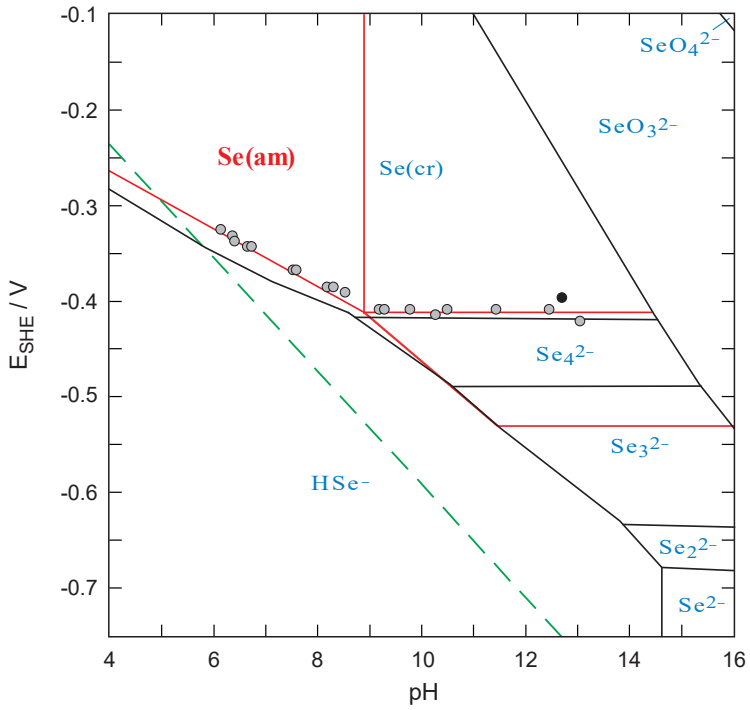

Fig. A2: The same Eh – pH predominance diagram of selenium as shown in Fig. A1, with interpretation of experimental data according to Iida et al. (2010) (red lines).

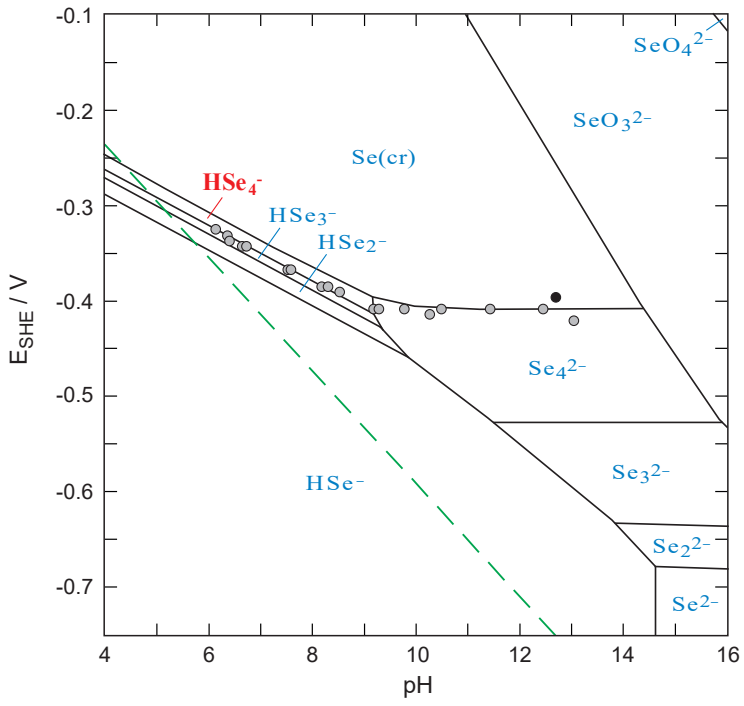

Fig. A3: The Eh – pH predominance diagram of selenium showing the re-interpretation of the experimental results of Iida et al. (2010) by the present author in terms of the formation of HSe_4^-; lines for HSe_3^- and HSe_2^- are guesses.

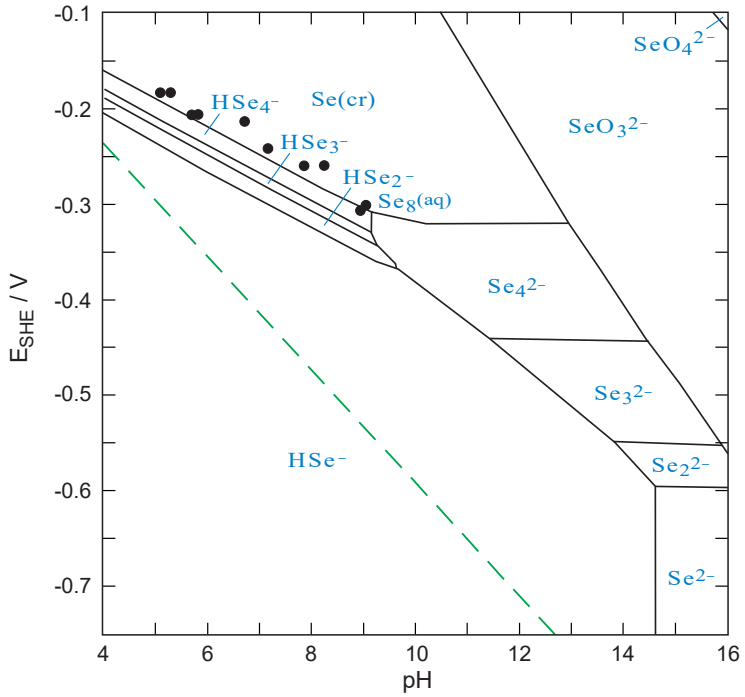

Fig. A4: The Eh – pH predominance diagram of selenium showing the re-interpretation of the experimental results of Iida et al. (2010) (black circles: from undersaturation) by the present author for $[Se]_{total} = 3 \times 10^{-5}$ mol dm^{-3}.

A re-interpretation of the experimental data by the present author suggests that Iida et al. (2010) actually measured the protonation of a polyselenide, presumably

$$Se_4^{2-} + H^+ \rightleftharpoons HSe_4^-.$$

A preliminary fit of a conditional stability constant at ionic strength I = 0.1 mol dm^{-3} for the above equilibrium using the experimental data from Iida et al. (2010) is visualised in Fig. A3 and A4 for $[Se]_{total} = 2 \times 10^{-2}$ mol dm^{-3} and $[Se]_{total} = 3 \times 10^{-5}$ mol dm^{-3}, respectively. The lines drawn for HSe_3^- and HSe_2^- are based on pure guesses for the respective protonation equilibria, put somewhere "in between" the fitted constant for HSe_4^- and the know constant for HSe^-.

Furthermore, the experimental data of Iida et al. (2010) and their re-interpretation by the present author indicate an upper limit for the solubility of Se(cr) $\rightleftharpoons$ Se(aq) of Se(aq) < 10^{-5} mol dm^{-3}.

However, all these results need confirmation.

Van Es, E., Hinchliff, J., Felipe-Sotelo, M., Milodowski, A.E., Field, L.P., Evans, N.D.M. & Read, D. (2015): Retention of Chlorine-36 by a cementitious backfill. Mineralogical Magazine 79, 1297-1305.

In this paper we find data from radial diffusion experiments which have been carried out to assess the migration of ^{36}Cl, as chloride, through a cementitious backfill material, the so-called Nirex Reference Vault Backfill (NRVB). Further experiments in the presence of cellulose degradation products (CDP) were performed to assess the effect of organic ligands on the extent and rate of chloride diffusion.

On a first glimpse this publication seems to provide information about the retention of ^{36}Cl by a cementitious backfill. However, a detailed review of the paper revealed that due to unclear and contradictory experimental conditions no meaningful interpretation of the results is possible, not even in qualitative terms.

The decisive part of the description of experimental conditions reads like that (van Es et al. 2015): "The experiments were carried out with non-radioactive chloride (NaCl, Aldrich) carrier concentration between 10^{-4} and 10^{-1} mol dm^{-3} (after equilibration), containing 13 kBq ^{36}Cl tracer (Amersham International). Known concentrations of chloride were added to the central well (~ 1 cm^3 volume), which was then sealed and submerged in either NRVB-equilibrated water or a CDP solution. … For all experiments, the total volume of the system was 250 cm^3, of which 200 cm^3 correspond to the external solution and 50 cm^3 to the cylinder, the latter equates to 25 cm^3 pore volume, based on a volumetric porosity of 0.5. … The solution surrounding the NRVB cylinders was sampled periodically and ^{36}Cl activity measured by liquid scintillation counting".

First of all, the authors seemed not to be aware of the fact that NRVB equilibrated solutions and CDP solutions contain a background of non-radioactive chloride in the range of $0.4 – 1.2\times10^{-3}$ mol dm^{-3} and $0.6 – 2.5\times10^{-3}$ mol dm^{-3}, respectively, although these experimentally determined values have been published earlier by the same group (Tab. 1 in Felipe-Sotelo et al. 2014).

As a consequence, it is impossible to reach an equilibrium carrier concentration of 10^{-4} mol dm^{-3} (after equilibration in 225 cm^3 total volume) with the reported experimental set-up. By simple mass balance the background of non-radioactive chloride is always 4 to 25 times higher than the claimed carrier concentration.

Trying to understand whether and how the maximum carrier concentration has been reached is even more confusing.

The value "10^{-1} mol dm^{-3} (after equilibration)" cited above seems to be a typo error. In all other occurrences in the paper the value 3×10^{-1} mol dm^{-3} is given, e.g. in the figure caption of Fig.2 in van Es et al. (2015): "Breakthrough curves for ^{36}Cl at various carrier levels (NaCl $10^{-4} – 3 \times 10^{-1}$ mol dm^{-3}) in NRVB equilibrated water". And further in the text we find: "At a carrier concentration corresponding to seawater (3×10^{-1} mol dm^{-3}) …". So, we presume that they actually aimed at reaching an equilibrium carrier concentration of 0.3 mol dm^{-3} in 225 cm^3 total volume.

However, the experimental procedure to achieve this goal remains unclear. The sole information given is "known concentrations of chloride were added to the central well".

We assume that the authors followed the same procedure as described in their earlier paper (Felipe-Sotelo et al. 2014) where they added 0.15 mol dm^{-3} KI solution to the central well (assuming exactly 1.5 cm^3 volume) in order to reach 10^{-3} mol dm^{-3} non-radioactive I^- carrier in 225 cm^3 total volume after equilibration (a dilution factor of 150).

Hence, in order to reach an equilibrium concentration of 0.3 mol dm^{-3} NaCl in 225 cm^3 total volume we would have to add 1.5 cm^3 of a 45 mol dm^{-3} NaCl solution to the central well. This exceeds the solubility of NaCl by an order of magnitude. No clue is given in the paper that they added crystalline NaCl to the central well, and a simple mass calculation shows that even if they did, the claimed experimental set-up is hardly feasible: Assuming the same dilution factor of 150 as described by Felipe-Sotelo et al. (2014) we need 0.0675 mol NaCl in the 1.5 cm^3 volume of the central well. As the molecular weight of NaCl is 58.44 g mol^{-1} we have to add 3.94 g solid to the central well. The density of crystalline NaCl is 2.165 g cm^{-3}. Consequently, we would need 1.8 cm^3 for the NaCl solid alone, plus some volume for water to dissolve the radioactive tracer and to create a saturated NaCl brine. Did they drill a considerably larger well? Was solid NaCl added "stepwise"? What was the real initial condition of this experiment?

Finally, the authors solely measured the ^{36}Cl activity in the solution surrounding the NRVB cylinders, but they did not measure the concentration of non-radioactive chloride. Hence, we have no clue whether constant chloride concentrations have been reached, and at what levels.

So, in addition to unclear and contradicting initial conditions we have no boundary conditions. This renders any modelling attempt impossible. Even qualitative interpretations of the reported ^{36}Cl breakthrough curves remain highly speculative as they are based on guesses about experimental conditions.